



# LensVLM: Selective Context Expansion for Compressed Visual Representation of Text

Roy Xie<sup>1,2</sup>, Dan Friedman<sup>1</sup>, Donghan Yu<sup>1</sup>, Bowen Pan<sup>1</sup>, Christopher Fifty<sup>1</sup>, Jang-Hyun Kim<sup>1</sup>, Xianzhi Du<sup>1</sup>, Zhe Gan<sup>1</sup>, Vivek Rathod<sup>1</sup>, Bhuwan Dhingra<sup>1,2</sup>

<sup>1</sup>Apple, <sup>2</sup>Duke University

Vision Language Models (VLMs) offer the exciting possibility of processing text as rendered images, bypassing the need for tokenizing the text into long token sequences. Since VLM image encoders map fixed-size images to a fixed number of visual tokens, varying rendering resolution provides a fine-grained compression knob. However, accuracy deteriorates quickly as compression increases: characters shrink below the vision encoder’s effective resolution, making them indistinguishable. To address this, we propose LensVLM, an inference framework and post-training recipe that enables VLMs to scan compressed images, then selectively expand only the relevant images to their uncompressed form via learned tools. Building on Qwen3.5-9B-Base, LensVLM maintains accuracy comparable to the full-text upper bound at 4.3× effective compression and outperforms retrieval-based, text- and visual-compression baselines up to 10.1× effective compression across seven text QA benchmarks. LensVLM also generalizes to multimodal document and code understanding tasks, with the accuracy gain over baselines growing as compression increases. Our analysis validates this approach: training makes visual compression robust to rendering choices, and as compression grows the model increasingly relies on expanded content rather than unreliable visual reading. The analysis also yields practical tool-choice guidance: text expansion is preferable for rendered text, while high-resolution image expansion suits native documents whose layout cues carry task-relevant information.

**Correspondence:** [ruoyu.xie@duke.edu](mailto:ruoyu.xie@duke.edu)

**Code & Model:** <https://github.com/apple/ml-lensvlm>\*

**Date:** May 11, 2026

## 1 Introduction

A growing line of work treats text not as a sequence of subword tokens but as an image to be consumed by a vision-language model (VLM) (Cheng et al., 2025; Wei et al., 2025; Xing et al., 2025; Wang et al., 2026; Gao et al., 2026). Under certain rendering configurations, rendered text packs into far fewer visual tokens than its text counterpart. This is particularly appealing for long-context applications, since self-attention scales quadratically with sequence length and shorter sequences reduce both compute and memory (Vaswani et al., 2017; Tay et al., 2022).

One key advantage of this approach is the flexibility of visual tokenization, as compression options are limited in text space. Retrieval-augmented generation (Lewis et al., 2020) selects relevant passages for

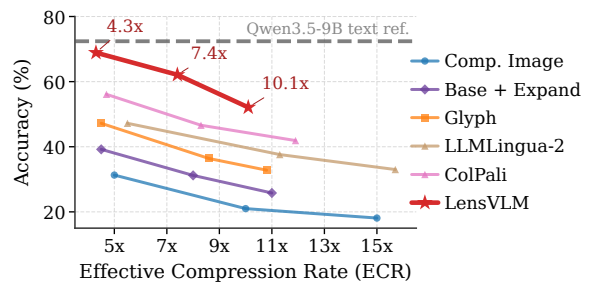


**Figure 1** Average QA accuracy vs. effective compression rate (ECR) across seven benchmarks. LENSVLM maintains accuracy comparable to the full-text upper bound at 4.3× ECR, resulting in the best accuracy–compression trade-off as visual fidelity degrades.

\* Under legal review and will be released soon.

the reader but commits a priori to what is retained and requires an offline index, whereas visual tokenization compresses all content while preserving global coverage (detailed comparison in §3.3). Token-pruning methods (Jiang et al., 2023; Pan et al., 2024) can drop tokens, but the compression is discrete and lossy with no way to recover pruned content. More fundamentally, changing text tokenization (e.g., longer subword units) requires vocabulary expansion and costly retraining, and the compression rate is fixed once the tokenizer is chosen. VLMs already process images and text natively, so the compression rate can be tuned continuously by adjusting rendering configuration, without retraining the tokenizer or the model.

We ask how far this idea can be pushed. Existing work invests heavily in improving VLMs’ reading ability (Cheng et al., 2025), but it degrades significantly as compression increases. Figure 1 compares different methods using the same Qwen3.5-9B-Base backbone except Glyph (GLM-4.1V-9B). The bottleneck is *fidelity*: as compression increases, rendered images shrink, characters become illegible, and the model has no way to recover the lost information. Past a certain compression rate, the pixels simply do not contain the bits.

Rather than asking the VLM to read perfectly at any compression, we introduce LensVLM<sup>1</sup>, an inference framework and post-training recipe that augments VLMs with tools to selectively expand parts of their visual context. The model first scans compressed images, then uses a learned tool to expand the relevant regions into uncompressed form (source text or high-resolution images). We argue that compression *should not be* a one-way lossy transform applied uniformly to the context; it *should be* a capability the model internalizes to undo when needed. Unlike retrieval methods that preprocess and index the entire context before any question, LensVLM takes compressed visual tokens as input and expands only the images the model selects on demand. To teach this behavior, we bootstrap supervision from synthetic tool-use traces generated with ground-truth evidence, then post-train via SFT followed by RL.

A comprehensive evaluation across text QA, multi-document understanding, and code understanding datasets shows that LensVLM pushes compression further than baselines, maintaining accuracy comparable to the full-text upper bound at 4.3× effective compression rate (ECR) and outperforming baselines up to 10.1× ECR across seven text QA benchmarks; ECR measures the total tokens the reader actually processes relative to the source token length (§3.2). Our analyses connect these gains to the design choices behind LensVLM. First, training makes visual compression robust to rendering choices, reducing an 18-point accuracy spread across rendering configurations to under 1 point (§5.1). Second, controlled tool variants show that the main bottleneck is access to readable evidence: chain-of-thought without tools does not improve accuracy, while returning source text or high-resolution images through the EXPAND tool does (§5.3). These variants also provide a practical tool choice: text is best for rendered text, while image zoom is better for native documents where layout and visual cues matter. Third, attention analysis shows that training redirects attention away from distractor images and toward the content returned by EXPAND, with this shift growing at higher compression and explaining why LensVLM’s advantage increases as visual fidelity decreases (§5.2).

## 2 Related Work

**Visual-Text Compression** A growing line of work compresses text by rendering it as images for VLMs. PIXEL (Rust et al., 2022) first showed that language modeling over rendered pixels is viable. Glyph (Cheng et al., 2025) extends this to long-context reasoning with optimized rendering layouts. VIST (Xing et al., 2025) introduce dual-path architectures that route distant context through a visual encoder while keeping nearby tokens as text. VTC-R1 (Wang et al., 2026) and AgentOCR (Feng et al., 2026) apply RL to learn what to render. In the text-only space, LLMingua (Jiang et al., 2023) and LLMingua-2 (Pan et al., 2024) prune tokens directly. Like these methods, we compress text into visual tokens; unlike them, LensVLM introduces an expansion tool to selectively decompress key sections of the input. Existing visual-text compression methods ask the model to answer from a fixed compressed view, so accuracy is bounded by what remains readable at that compression rate. LensVLM instead keeps the compressed view for global scanning and selectively expands relevant regions back to uncompressed form, pushing beyond the limits of visual reading.

**Tool-Augmented Reasoning and Document Understanding** A parallel line of work teaches VLMs to use visual tools (cropping, zooming, searching) via SFT and RL (Su et al., 2025; Zheng et al., 2025; Fan et al., 2025;

---

<sup>1</sup>The name reflects its lens-like ability to focus on compressed visual context and magnify selected regions.

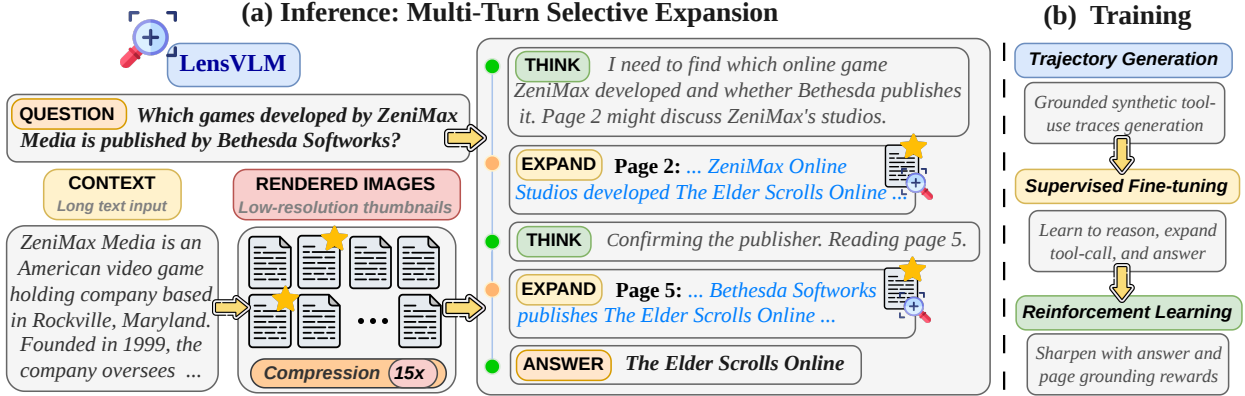


**Figure 2** Overview of LensVLM. (a) Text is rendered into compressed images and fed to the model, which interleaves reasoning with EXPAND tool to selectively recover relevant images in uncompressed form across multiple turns. (b) LensVLM is trained through a three-stage pipeline: hard examples are filtered from the base model, synthetic tool-use traces are generated for SFT, and RL further improves answer and tool-use correctness.

Wu et al., 2025), while retrieval-based document methods select relevant images before reasoning (Cho et al., 2024; Huang et al., 2025; Jain et al., 2025). In the document domain specifically, ARM-Thinker (Ding et al., 2025) combines image retrieval with cropping tools, and architectural methods compress document images at the feature level (Hu et al., 2025; Thapa et al., 2024). Similar to visual tool-use methods, we train tool-use through post-training; like retrieval methods, LensVLM selects which content to read. The key difference is twofold: (1) prior tool-use work, including document methods like ARM-Thinker and DeepEye, use tools to resolve visual ambiguity within a *given* image and documents, whereas in LensVLM the images are a deliberate compression of text; and (2) standard retrieval pipelines preprocess and commit to a fixed selection before reasoning begins (Xie et al., 2025), whereas LensVLM selects which compressed regions to expand conditioned on evolving multi-turn context.

### 3 Method

Figure 2 shows an overview of LensVLM. Text is rendered into compressed images; the model selectively expands specific images into uncompressed form via EXPAND. This behavior is learned from synthetic tool-use traces, followed by post-training via SFT and RL.

#### 3.1 Compression: Rendering Text as Images

The compression step uses a deterministic renderer  $f$  to convert a text input  $\mathcal{D}$  of  $N$  tokens into a sequence of  $K$  images  $\mathcal{V} = f(\mathcal{D}) = (v_1, \dots, v_K)$ . The renderer is parameterized by a rendering configuration (font, geometry, line spacing) that fixes the text capacity per image. A vision encoder then tokenizes each image  $v_k$  into  $n_k$  visual tokens, yielding total  $\sum_{k=1}^K n_k$  visual tokens fed to the language model. We define the *input compression rate* (ICR)

$$C_{\text{in}} = \frac{N}{\sum_{k=1}^K n_k}, \quad (3.1)$$

the ratio of text tokens to visual tokens consumed. At  $C_{\text{in}} = 1$  the model sees one visual token per text token, while  $C_{\text{in}} \gg 1$  packs more than one text token into a visual token. Higher compression reduces image dimensions and visual tokens per image. Details and examples are in Appendix 7.1.

#### 3.2 Selective Expansion via Tool Use

The model manages its context through a learned tool  $\text{EXPAND}(k)$  that recovers selected compressed images into uncompressed form. Given an image index  $k$ ,  $\text{EXPAND}(k)$  returns a representation  $\tau_k$  of the corresponding

source content: depending on the task,  $\tau_k$  may be source text, OCR-extracted text, or a high-resolution image (different variants are compared in §5.3). Let  $\pi_\theta$  denote the VLM policy with parameters  $\theta$ . At inference, the model sees all  $K$  images alongside a question  $q$  and samples a multi-turn trajectory:

$$y \sim \pi_\theta(\cdot | \mathcal{V}, q), \quad (3.2)$$

where the trajectory  $y = (r_1, k_1, \tau_{k_1}, \dots, r_M, k_M, \tau_{k_M}, a)$  is a sequence of reasoning steps  $r_t$ , tool calls  $\text{EXPAND}(k_t)$  with  $k_t \in \{1, \dots, K\}$ , and their responses  $\tau_{k_t}$  appended to the context, terminating with a final answer  $a$  after  $M \leq T$  tool calls. Each turn expands exactly one image; when multiple images are needed, the model expands them sequentially across turns, conditioning each selection on previously expanded content.

**Selection-then-Expansion** The tool introduces no additional information beyond  $\mathcal{D}$ ; it re-presents selected regions in a form the model can read more reliably, recovering information that may be inaccessible after visual compression. Our hypothesis is that compressed images preserve enough coarse evidence for the model to identify likely answer-containing regions, even when they do not preserve the token-level content needed for extraction (detailed analysis in Appendix 8). Building on this notion, LensVLM teaches the model to use compressed images for selection, then invoke EXPAND to access the selected region in uncompressed form. We evaluate this hypothesis empirically: as visual reading degrades under stronger compression, selective expansion remains effective (§4.2), with trained selection accuracy degrading far more gracefully than visual reading across compression rates (Appendix 8).

This selection-then-expansion framework is not tied to a particular backbone: it can be applied to frontier VLMs through prompting alone (Appendix 9), while our post-training recipe teaches a compact 9B model to execute the same behavior end-to-end.

**Effective Compression** Different methods compress the same source text into different numbers of reader-visible tokens, due to differences in vision encoders, retrieval budgets, or tool-call responses. To compare methods fairly, we use the *effective compression rate* (ECR): the ratio of the original text length to the total number of tokens actually processed by the model,

$$C_{\text{eff}} = \frac{N}{T_{\text{reader}}}, \quad (3.3)$$

where  $N$  is the source text token count and  $T_{\text{reader}}$  is the total reader input tokens. For LensVLM,  $T_{\text{reader}}$  includes both the initial compressed visual tokens and any tokens appended by EXPAND calls, so  $C_{\text{eff}} \leq C_{\text{in}}$ . For visual reading without tools,  $C_{\text{eff}} = C_{\text{in}}$ . We report ECR for all methods; per-method ECR details are in Appendix 11. Efficiency analysis in Appendix 10.

### 3.3 Design Rationale: Retrieval vs. Compression

Retrieval is the dominant practical alternative for reducing reader input in long-context QA, and EXPAND can be viewed as a learned retriever in which the VLM itself acts as indexer, selector, and reader in a single end-to-end model. The two paradigms, however, differ along three axes. *Compression mechanism*: retrieval reduces coverage by selecting the top- $\lceil K/C_{\text{in}} \rceil$  of  $K$  images at rate  $C_{\text{in}} \times$  and discarding the rest, whereas LensVLM reduces visual fidelity, rendering all images at lower resolution to preserve global overview. *Preprocessing*: retrieval requires an offline index building on the full context (source text or high-resolution images) with chunking granularity and top- $k$  fixed a priori, while LensVLM needs only CPU rendering and makes EXPAND selections dynamically at inference, conditioned on the question and prior expansions across turns. *Regime*: retrieval is preferable when evidence is concentrated in a few chunks and indexing cost amortizes across many queries; visual compression is preferable when evidence may be distributed (so top- $k$  risks dropping relevant images), when the source is natively visual with layout cues that text retrievers cannot preserve, or when offline indexing is impractical. The two are complementary: a cheap retriever could prune grossly irrelevant chunks before rendering. Empirical comparisons are in §5.6.

### 3.4 Data Construction

We construct training data by rendering text from several text QA datasets into images at a fixed ICR and tracking character-level answer spans through pagination to identify the ground-truth evidence images

$E^* \subseteq \{1, \dots, K\}$  for each sample. Not all samples require tool use: some can be answered directly from the compressed images. Following Zheng et al. (2025), we classify each sample as *easy* (base model answers correctly without tools) or *hard* (tool use needed), determined by running the base VLM on each sample (Appendix 12.2).

For each hard sample, a synthesis model (Qwen3.5-397B) receives the question  $q$ , the evidence in its uncompressed form, and the gold answer  $a^*$  to generate a synthetic multi-turn trajectory:

$$y^* \sim \pi_{\text{synth}}(\cdot \mid q, \mathcal{D}_{E^*}, a^*), \quad (3.4)$$

producing chain-of-thought reasoning interleaved with  $|E^*|$  EXPAND calls. Direct distillation from frontier models is not viable: they produce noisy, hallucination-filled traces when reasoning over highly compressed images, and the EXPAND behavior is not native to these models. Synthesis sidesteps both issues by providing evidence together with the known answer, reducing the task to generating a coherent reasoning and tool-use trajectory rather than solving visual comprehension under degraded conditions (examples in Appendix 18).

### 3.5 Post-Training

**Supervised Fine-Tuning** Initializing  $\pi_\theta$  from a pretrained VLM and decomposing each synthetic trajectory  $y^*$  from Equation (3.4) into its  $L$  tokens  $(y_1^*, \dots, y_L^*)$ , the training objective is to minimize the autoregressive loss over  $\pi_\theta$  produced tokens:

$$\mathcal{L}_{\text{SFT}}(\theta) = - \sum_{i \in \mathcal{A}} \log \pi_\theta(y_i^* \mid \mathcal{V}, q, y_{<i}^*), \quad (3.5)$$

where  $\mathcal{A} \subseteq \{1, \dots, L\}$  indexes tokens produced by  $\pi_\theta$ . The expanded tool responses  $\tau_{k_i}$  remain in the context as inputs but are masked from the loss (Jin et al., 2025). We train on the hard subset only since easy samples do not benefit from tool use and including them dilutes the signal. Following Sun et al. (2026), we freeze the vision encoder and visual projector and update only the language model parameters during both SFT and RL (see Appendix 7.2 for details). We denote the resulting parameters  $\theta_{\text{SFT}} \in \arg \min_\theta \mathcal{L}_{\text{SFT}}(\theta)$ , which initialize the RL stage below.

**Reinforcement Learning** SFT initializes the model with synthetic tool-use trajectories, but these traces reflect the teacher policy distribution. To address this mismatch, we therefore use on-policy RL to let the model learn under its own policy. Starting from the SFT checkpoint, we initialize  $\theta \leftarrow \theta_{\text{SFT}}$  and optimize  $\pi_\theta$  on a training distribution  $\mathcal{P}$  over  $(\mathcal{V}, q, a^*)$  tuples (images, question, gold answer), maximizing the expected episode reward:

$$\mathcal{J}(\theta) = \mathbb{E}_{(\mathcal{V}, q, a^*) \sim \mathcal{P}, y \sim \pi_\theta(\cdot \mid \mathcal{V}, q)} [R(y, a^*)], \quad (3.6)$$

where  $y$  is a model trajectory. Since ground-truth evidence images are not observed during RL, the reward uses only final-answer feedback and an answer-gated tool-use bonus:

$$R(y, a^*) = 0.7 \cdot c + 0.3 \cdot c \cdot u, \quad (3.7)$$

where  $c = \text{acc}(y, a^*) \in \{0, 1\}$  is answer correctness using a LLM judge and  $u = \mathbb{1}[\text{EXPAND} \in y]$  indicates whether the trajectory uses the tool. Following Zheng et al. (2025), the tool-use bonus is gated by answer correctness. This incentivizes tool use even when the answer could be obtained without it; we accept this bias because the cost of an unnecessary EXPAND call is small (one extra image) relative to the cost of not reading when needed (a wrong answer). To bound this cost, we cap each episode at  $T=6$  turns, hard-limiting EXPAND calls per trajectory and preventing runaway tool spam. Empirically, degenerate behavior does not emerge within this cap: the model averages only 1.3 EXPAND calls per trajectory (§15.3). We use DAPO (Yu et al., 2025) as the RL algorithm.

## 4 Experiments

### 4.1 Experimental Setup

**Datasets & Models** We train on NQ (Kwiatkowski et al., 2019), HotpotQA (Yang et al., 2018), MuSiQue (Trivedi et al., 2022), and HELMET (Yen et al., 2025). In addition to the above benchmarks, we also

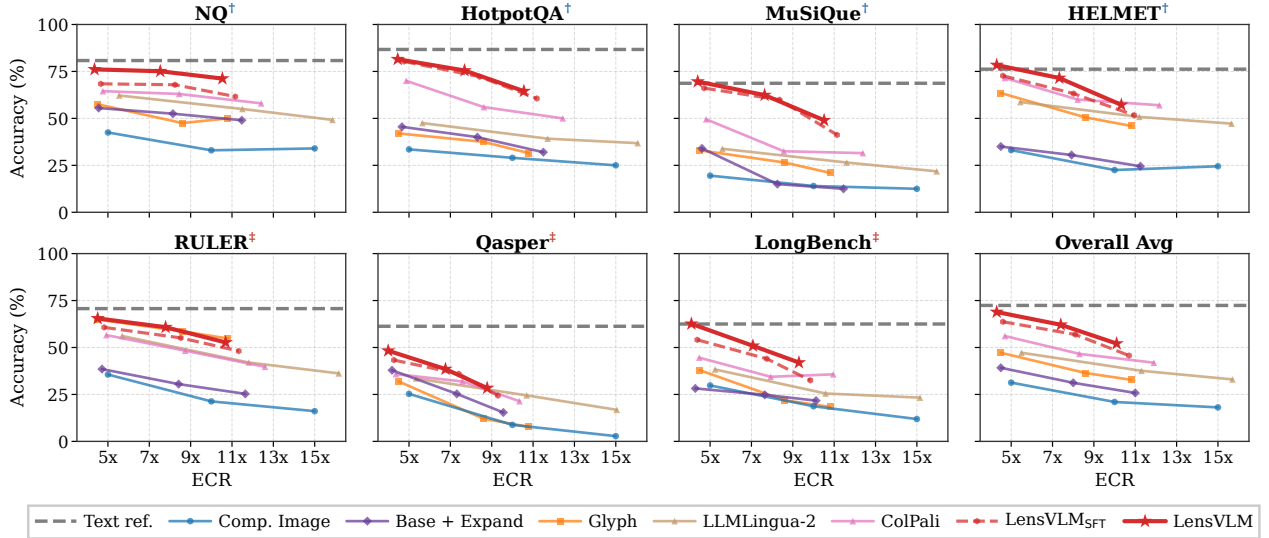


**Figure 3** LensVLM outperforms or matches all baselines at every compression rate on both in-domain ( $\dagger$ ) and out-of-domain ( $\ddagger$ ) benchmarks. All methods share the same Qwen3.5-9B-Base reader except Glyph (GLM-4.1V-9B).

evaluate on out-of-distribution benchmarks: Qasper (Dasigi et al., 2021), LongBench v1 (Bai et al., 2024), and RULER (Hsieh et al., 2024). We evaluate on datapoints with fewer than 32K text tokens; for RULER and LongBench we use the subsets that fall within this budget (Appendix 12). We also evaluate on guaranteed-unseen post-cutoff data to check pre-training contamination (Table 5; details in Appendix 14). LensVLM is built on Qwen3.5-9B-Base (Qwen Team, 2026), a VLM with native image-text support whose vision encoder maps each image into a fixed number of visual tokens (72, 48, or 24 at three ICR levels). We train a single LensVLM policy across all compression rates. Qwen3.5-397B is used as the LLM judge (Appendix 7.4).

**Baselines** We compare LensVLM against various baselines. As an upper bound, **Text** feeds the entire document as raw text tokens to the backbone model. **Comp. Image** renders all text as compressed images and feeds them to the backbone model. **Base + Expand**, uses the backbone model to read compressed images and predict the evidence image and then expands it. **LLMLingua-2** (Pan et al., 2024) prunes tokens to match the target compression rate. For image retrieval, we compare with **ColPali** (Faysse et al., 2024), the state-of-the-art visual retriever over rendered images. Retrieved and the pruned tokens are then fed into the backbone model. All methods above share the same backbone (Qwen3.5-9B-Base) for fair comparison. For model-based methods, we evaluate **Glyph** (Cheng et al., 2025), a strong same size visual-compression model (GLM-4.1-9B). We analyze broader RAG baselines separately in §5.6 and discuss additional text and visual compression alternatives and per-baseline compression setup in Appendix 11.

**Evaluation Metrics** We report QA accuracy as the primary metric, computed by a LLM judge for semantically equivalent answers. For each benchmark, we report the unweighted macro-average accuracy across constituent datasets. We also report selection accuracy (Sel. Acc.), the fraction of trajectories where at least one EXPAND call selects a ground-truth evidence image. We report ECR (§3.2) for fair comparison for all methods. Evaluation uses the same turn budget as training ( $T=6$ ).

## 4.2 Main Results

**Text QA Under Compression** Figure 3 shows accuracy and ECR trade-offs. Naive visual reading fails: at 5 $\times$ , compressed image drops to 31.3% against the 72.4% text upper bound. Glyph partially recovers but is sensitive to different rendering configuration and compression rate (Cheng et al., 2025). Simply predicting and expanding an image with the untrained base model (Base + Expand) yields 39.2% at 5 $\times$ , showing that the tool-use augmentation itself provides value even without training. LensVLM maintains 68.9% at 5 $\times$  (ECR 4.3 $\times$ ), and achieves the best accuracy-compression trade-off at all three ICRs. For retrieval baselines, ECR

**Table 1** Code understanding generalization. LensVLM transfers tool-use to code without code-specific training.

Method	5×	10×	15×
Text	65.6	65.6	65.6
Comp. Image	26.7	6.1	3.2
Glyph	31.8	9.7	7.0
LensVLM	<b>38.1</b>	<b>26.1</b>	<b>20.0</b>
<i>ECR</i>	3.2×	6.3×	8.2×
<i>Sel. Acc.</i>	55.5	43.5	31.7

**Table 2** Document QA task. The zoom tool outperforms OCR by preserving layout and visual cues.

Method	5×	10×	15×
Original Image	57.5	57.5	57.5
Comp. Image	<b>51.2</b>	40.3	31.1
LensVLM + OCR	45.8	38.7	32.1
<i>ECR</i>	5.0×	9.4×	13.5×
<i>Sel. Acc.</i>	51.2	39.5	33.3
LensVLM + Zoom	50.5	<b>46.6</b>	<b>41.9</b>
<i>ECR</i>	4.2×	7.7×	10.3×
<i>Sel. Acc.</i>	51.5	42.0	36.2

reflects only the reader’s input budget; the indexing pass over the full context is paid offline (§3.3). SFT alone lifts accuracy from 31.3% to 63.7%, and RL sharpens image selection and reasoning over expanded content, reaching 76.8%/71.0%/52.1% selection accuracy at 5×/10×/15×. We further analyze each training stage in Appendix 15.1. Full per-dataset QA results are in Table 11 (Appendix 13), selection accuracy in Table 12 (Appendix 13), and a contamination-free replication on post-cutoff data confirms comparable gains in Section 5.5.

**Zero-Shot Transfer to Code** To test whether LensVLM generalizes beyond natural-language text, we evaluate on two coding benchmarks: RepoQA (Liu et al., 2024), a function retrieval task over long code repositories from 6 languages, and CodeQueries (Sahu et al., 2024), a QA task over code. Code is rendered using the same pipeline (§3.1). Table 1 shows that LensVLM improves from Comp. Image and outperforms Glyph at every compression level, demonstrating that tool-use transfers to code *without* code-specific training. The resulting ECRs are lower on these benchmarks because context lengths are short; LensVLM benefits most from longer contexts where the fixed tool-call cost amortizes over more visual tokens. More details are in Appendix 16.2.

**Document Understanding with Visual Tools** To test whether our method applies to native multimodal document images, we train two variants of LensVLM with the same training procedure and evaluate on MMLongBench-Doc (Ma et al., 2024) (a multi-image document QA benchmark containing long PDFs): one with an OCR text extraction tool (PaddleOCR-VL (Cui et al., 2026)) and one with an image zoom tool (returning a high-resolution image). We compare both against the base VLM reading original and compressed images (Table 2). At 5×, compressed images remain largely readable and the base model outperforms both zoom and OCR tools, as the base model may also benefit from pretraining exposure to this popular benchmark (Deng et al., 2024). The advantage of tool-use emerges as compression increases: at 15× the zoom tool reaches 41.9% versus 31.1% for the base model. The OCR tool also surpasses the base at 15×, but lags behind zoom because extracted text discards layout and visual cues that the zoom tool preserves. However, this gain comes at a compression cost: the zoom tool’s ECR is lower than OCR tool as high-resolution images cost more than OCR text. More details are in Appendix 16.1.

## 5 Analysis & Discussion

### 5.1 Training Erases Rendering Sensitivity

The optimal rendering configuration for text-to-image compression is largely under-explored; finding one often requires exhaustive search over many rendering parameters (Cheng et al., 2025; Gao et al., 2026). As shown in Figure 4, even at roughly matched compression, the base model remains highly sensitive to rendering: accuracy varies by 32 points across 20 configurations, including an 18-point gap within a single font group.

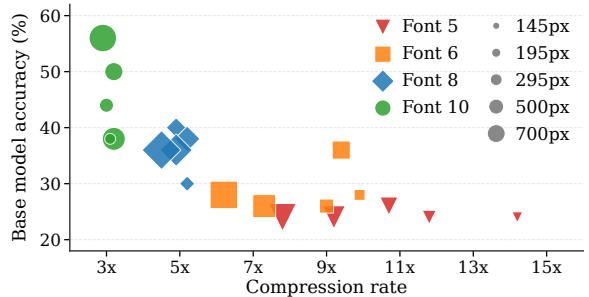


**Figure 4** The base model is highly sensitive to rendering configuration: accuracy spans a 32-point range across 20 configurations.

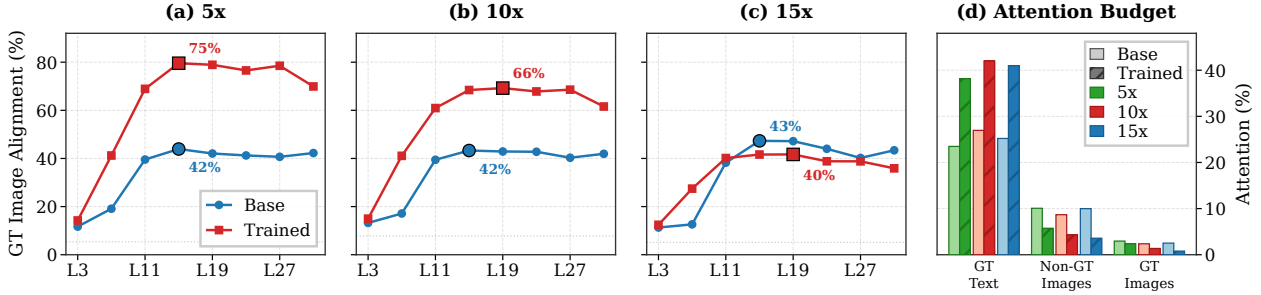


**Figure 5** Attention analysis across compression rates. (a–c) The base model localizes evidence images above chance; post-training sharpens this into predictions. (d) After training, the model redirects attention from distractor images to expanded text, increasingly so at higher compression.

To test whether training reduces this sensitivity, we train three model variants with the same 10pt font on matched-compression configurations: wide (700px), medium (295px), and tall (145px), all at  $\sim 3\times$  compression (Table 3) using  $\sim 40K$  matched samples. Before training (Base), accuracy drops monotonically from 56.2% to 38.2% as images narrow. After training, all three converge to similar performance, reducing the configuration gap from 18.0 to 0.5 points. This insensitivity likely arises from two sources: trained models specialize to their own rendering configuration, and the text returned by the tool is invariant to how the image was rendered, letting the model rely on expanded content rather than visual legibility (Section 5.2). We do not separate these effects here, but both lead to the same practical conclusion: training removes the need for expensive rendering search, making the configuration a flexible design choice rather than a hyperparameter to optimize.

**Table 3** Rendering configuration ablation at matched  $\sim 3\times$  compression. LensVLM eliminates sensitivity.

	700px	295px	145px	$\Delta$
CR	2.9 $\times$	3.2 $\times$	3.1 $\times$	
Base	56.2	50.7	38.2	18.0
LensVLM	70.3	70.4	70.8	0.5

## 5.2 Attention Analysis

To understand what post-training changes, we analyze attention patterns on test samples at three compression rates (Figure 5; setup details in Appendix 17.1). For each decode step, we compute per-image attention scores by summing head-averaged attention within each image’s visual-token range. Panels (a–c) plot the *GT-alignment rate*, the position-debiased fraction of samples whose peak-attention image is a GT evidence image, across the 8 standard-attention layers of Qwen3.5-9B for Base and Trained at each compression preset. Even the base model localizes evidence images well at every compression rate, consistent with the retrieval-head phenomenon in text-only LLMs (Wu et al., 2024). Training sharpens this diffuse signal into confident predictions at 5 $\times$  and 10 $\times$  where text remains readable, but cannot improve alignment at 15 $\times$  when the visual signal itself is depleted. Panel (d) clarifies how this change is used by showing the *attention budget*, the fraction of total attention assigned to each input segment. After training, the model allocates less attention to images overall, suppresses distractor images more than GT images, and redirects attention to the tool response. This evidence-focused shift becomes stronger as compression increases (full breakdown in Appendix 17.2), explaining why tool-mediated expansion becomes more valuable as visual fidelity degrades.

## 5.3 Tool Modality: Text vs. Image

We trained five model variants with  $\sim 40K$  matched samples differing only in what the model receives after calling EXPAND: (1) no tool access with a direct answer, (2) no tool access with reasoning traces, (3) OCR-extracted text from high-resolution rendered image, (4) original text, and (5) a high-resolution version of the selected image (Figure 6). Three findings stand out. *First*, the bottleneck is information access, not reasoning: chain-of-thought without tool access provides no benefit over direct answers, as reasoning over illegible images might introduce noise. *Second*, original text is the best tool response at every compression

level, which is expected. When the original text is unavailable (e.g., multimodal documents), OCR achieves similar performance, making it a practical substitute. *Third*, image zoom consistently underperforms both text tools on rendered text because text tokens provide higher fidelity than visual tokens of the same content. However, on native multimodal document images (Table 2) the ranking reverses: the zoom tool outperforms text tool because text tool discards layout and visual structure that the high-resolution image preserves.

#### 5.4 Effect of Model Scale

We train LensVLM with three size variants: 2B, 4B, and 9B, to measure the scale effect (Table 4). The 2B model learns the tool-call syntax, but its QA accuracy remains low even after training, indicating that stronger visual understanding is needed. The 4B model achieves moderate selection accuracy (59.1%), but QA accuracy plateaus at 56.3%, suggesting that understanding the expanded content becomes the bottleneck. In contrast, the 9B model supports the full agentic flow, with both visual grounding and text comprehension reaching effective levels. Overall, tool-augmented visual QA appears to require sufficient capacity for visual understanding, multi-step planning, and reading comprehension; smaller models may lack headroom for these combined demands.

#### 5.5 Contamination-Free Evaluation

Pre-training contamination is partially mitigated by construction: although popular source QA datasets may overlap with pre-training data, our rendered-image inputs are newly generated and therefore unlikely to have been seen during pre-training. To control for contamination more directly, we build a guaranteed-unseen test bed from PubMed Central data published *after* Qwen3.5’s pre-training cutoff (February 16, 2026), post-train a fresh model on this corpus, and evaluate it on a held-out test split (Table 5; details in Appendix 14). The pattern *mirrors* our main results: LensVLM gains +39.7 points on average across three ICRs, with the largest gains at high compression.

#### 5.6 Empirical Comparison with Retrieval

Table 6 compares LensVLM with representative text and visual retrievers under the same reader (§3.3 for the conceptual comparison). To match each compression level, retrieval selects the top- $\lceil K/C_{in} \rceil$  pages per document (see Appendix 11 for how compression levels map to retrieval top- $k$ ). BM25 is already strong

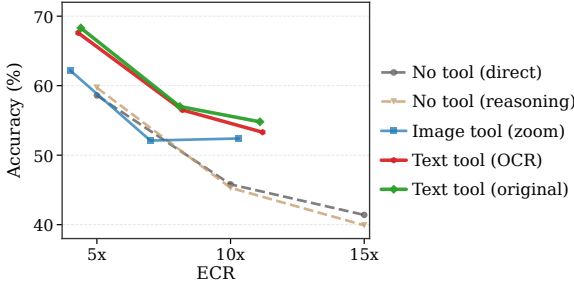


**Figure 6** Tool modality comparison. Original text outperforms OCR and image zoom; chain-of-thought without tools provides no benefit.

**Table 4** Effect of model scale. Tool-use behavior emerges only at 9B, where both image selection and QA accuracy reach effective levels.

Size	Stage	QA Acc.	Sel. Acc.
2B	Base	13.2	–
	LensVLM	45.5	49.4
4B	Base	25.7	–
	LensVLM	56.3	59.1
9B	Base	31.3	–
	LensVLM	<b>68.9</b>	<b>76.8</b>

**Table 5** Contamination-free training and evaluation on post-cutoff dataset. LensVLM’s gains hold on guaranteed-unseen data.

Method	5×	10×	15×
Text	92.1	92.1	92.1
Comp. Image	39.5	25.5	16.3
LensVLM	<b>86.8</b>	<b>60.0</b>	<b>53.7</b>
<i>ECR</i>	4.0×	7.9×	10.4×
<i>Sel. Acc.</i>	80.7	59.4	48.8

**Table 6** LensVLM vs. retrieval baselines. LensVLM outperforms or matches all retrievers at every compression level using only CPU preprocessing. C=CPU, G=GPU.

Method	Preproc.	Accuracy		
<i>Text retrieval</i>				
BM25	Idx <sup>C</sup>	<b>top-5</b>	<b>top-3</b>	<b>top-2</b>
		62.5	55.7	50.8
BGE-M3	Idx+Emb <sup>C+G</sup>	65.1	57.1	51.9
Jina-v4	Idx+Emb <sup>C+G</sup>	64.9	57.9	<b>52.1</b>
Qwen3-Emb	Idx+Emb <sup>C+G</sup>	64.4	56.5	51.1
<i>Visual retrieval</i>				
ColPali	Idx+Emb <sup>C+G</sup>	<b>top-5</b>	<b>top-3</b>	<b>top-2</b>
		56.1	46.6	41.9
Jina-v4-MM	Idx+Emb <sup>C+G</sup>	63.7	54.6	50.3
<i>Text-visual compression (ours)</i>				
		5×	10×	15×
LensVLM <sub>SFT</sub>	Rend. <sup>C</sup>	63.7	56.9	45.7
LensVLM	Rend. <sup>C</sup>	<b>68.9</b>	<b>62.1</b>	<b>52.1</b>

(62.5% at 5 $\times$ ); embedding retrievers improve slightly, while visual retrievers (ColPali, Jina-v4-MM) fall in a similar range. LensVLM matches or exceeds every retrieval baseline at every compression level. The *Preproc.* column highlights the structural cost: embedding retrievers require a GPU embedding pass over the full context at index time, whereas LensVLM requires only CPU rendering. We further analyze the selection mechanism through oracle ablations in Appendix 15.2.

## 6 Conclusion

We presented LensVLM, an inference framework and post-training recipe that enhances visual text compression by enabling VLMs to selectively expand compressed images. Across seven text QA benchmarks, LensVLM maintains performance near the full-text upper bound at 4.3 $\times$  effective compression, outperforms baselines up to 10.1 $\times$ , and generalizes to documents and code. Our analysis shows that training reduces sensitivity to rendering, that information access is the main bottleneck, and that models increasingly rely on tool-mediated expansion as compression grows.

## References

- Sandhini Agarwal, Lama Ahmad, Jason Ai, Sam Altman, Andy Applebaum, Edwin Arbus, Rahul K Arora, Yu Bai, Bowen Baker, Haiming Bao, et al. gpt-oss-120b & gpt-oss-20b model card. *arXiv preprint arXiv:2508.10925*, 2025.
- Reza Yazdani Aminabadi, Samyam Rajbhandari, Ammar Ahmad Awan, Cheng Li, Du Li, Elton Zheng, Olatunji Ruwase, Shaden Smith, Minjia Zhang, Jeff Rasley, et al. Deepspeed-inference: enabling efficient inference of transformer models at unprecedented scale. In *SC22: International Conference for High Performance Computing, Networking, Storage and Analysis*, pages 1–15. IEEE, 2022.
- Anthropic. Introducing Claude Sonnet 4.6. <https://www.anthropic.com/news/claude-sonnet-4-6>, 2026. Accessed: 2026-05-01.
- Yushi Bai, Xin Lv, Jiajie Zhang, Hongchang Lyu, Jiankai Tang, Zhidian Huang, Zhengxiao Du, Xiao Liu, Aohan Zeng, Lei Hou, Yuxiao Dong, Jie Tang, and Juanzi Li. LongBench: A bilingual, multitask benchmark for long context understanding. In *Proceedings of the 62nd Annual Meeting of the Association for Computational Linguistics*, 2024.
- Jiale Cheng, Yusen Liu, Xinyu Zhang, Yulin Fei, Wenyi Hong, Ruiliang Lyu, Weihang Wang, Zhe Su, Xiaotao Gu, Xiao Liu, Yushi Bai, Jie Tang, Hongning Wang, and Minlie Huang. Glyph: Scaling context windows via visual-text compression. *arXiv preprint arXiv:2510.17800*, 2025.
- Jaemin Cho, Debanjan Mahata, Ozan Irsoy, Yujie He, and Mohit Bansal. M3docrag: Multi-modal retrieval is what you need for multi-page multi-document understanding. *arXiv preprint arXiv:2411.04952*, 2024.
- Cheng Cui, Ting Sun, Suyin Liang, Tingquan Gao, Zelun Zhang, Jiaxuan Liu, Xueqing Wang, Changda Zhou, Hongen Liu, Manhui Lin, Yue Zhang, Yubo Zhang, Yi Liu, Dianhai Yu, and Yanjun Ma. Paddleocr-vl-1.5: Towards a multi-task 0.9b vlm for robust in-the-wild document parsing, 2026. URL <https://arxiv.org/abs/2601.21957>.
- Pradeep Dasigi, Kyle Lo, Iz Beltagy, Arman Cohan, Noah A. Smith, and Matt Gardner. A dataset of information-seeking questions and answers anchored in research papers. In Kristina Toutanova, Anna Rumshisky, Luke Zettlemoyer, Dilek Hakkani-Tur, Iz Beltagy, Steven Bethard, Ryan Cotterell, Tanmoy Chakraborty, and Yichao Zhou, editors, *Proceedings of the 2021 Conference of the North American Chapter of the Association for Computational Linguistics: Human Language Technologies*, pages 4599–4610, Online, June 2021. Association for Computational Linguistics. doi: 10.18653/v1/2021.naacl-main.365. URL <https://aclanthology.org/2021.naacl-main.365/>.
- Chunyan Deng, Yilun Zhao, Xiangru Tang, Mark Gerstein, and Arman Cohan. Investigating data contamination in modern benchmarks for large language models. In *Proceedings of the 2024 Conference of the North American Chapter of the Association for Computational Linguistics: Human Language Technologies (Volume 1: Long Papers)*, pages 8706–8719, 2024.
- Shengyuan Ding, Xinyu Fang, Ziyu Liu, Yuhang Zang, Yuhang Cao, Xiangyu Zhao, Haodong Duan, Xiaoyi Dong, Jianze Liang, Bin Wang, Conghui He, Dahua Lin, and Jiaqi Wang. Arm-thinker: Reinforcing multimodal generative reward models with agentic tool use and visual reasoning, 2025. URL <https://arxiv.org/abs/2512.05111>.
- Yue Fan, Xuehai He, Diji Yang, Kaizhi Zheng, Ching-Chen Kuo, Yuting Zheng, Sravana Jyothi Narayanaraju, Xinze Guan, and Xin Eric Wang. Grit: Teaching mllms to think with images. *arXiv preprint arXiv:2505.15879*, 2025.

- Manuel Faysse, Hugues Sibille, Tony Wu, Bilel Omrani, Gautier Viaud, Céline Hudelot, and Pierre Colombo. ColPali: Efficient document retrieval with vision language models. *arXiv preprint arXiv:2407.01449*, 2024.
- Lang Feng, Fuchao Yang, Feng Chen, Xin Cheng, Haiyang Xu, Zhenglin Wan, Ming Yan, and Bo An. Agentocr: Reimagining agent history via optical self-compression. *arXiv preprint arXiv:2601.04786*, 2026.
- Yonghan Gao, Zehong Chen, Lijian Xu, Jingzhi Chen, Jingwei Guan, and Xingyu Zeng. Zerosense: How vision matters in long context compression. *arXiv preprint arXiv:2603.11846*, 2026.
- Cheng-Ping Hsieh, Simeng Sun, Samuel Kriman, Shantanu Acharya, Dima Rekesh, Fei Jia, Yang Zhang, and Boris Ginsburg. Ruler: What’s the real context size of your long-context language models? *arXiv preprint arXiv:2404.06654*, 2024.
- Anwen Hu, Haiyang Xu, Liang Zhang, Jiabo Ye, Ming Yan, Ji Zhang, Qin Jin, Fei Huang, and Jingren Zhou. mPLUG-DocOwl2: High-resolution compressing for OCR-free multi-page document understanding. In Wanxiang Che, Joyce Nabende, Ekaterina Shutova, and Mohammad Taher Pilehvar, editors, *Proceedings of the 63rd Annual Meeting of the Association for Computational Linguistics (Volume 1: Long Papers)*, pages 5817–5834, Vienna, Austria, July 2025. Association for Computational Linguistics. ISBN 979-8-89176-251-0. doi: 10.18653/v1/2025.acl-long.291. URL <https://aclanthology.org/2025.acl-long.291/>.
- De-An Huang, Subhashree Radhakrishnan, Zhiding Yu, and Jan Kautz. Frag: Frame selection augmented generation for long video and long document understanding. *arXiv preprint arXiv:2504.17447*, 2025.
- Chelsi Jain, Yiran Wu, Yifan Zeng, Jiale Liu, Shengyu Dai, Zhenwen Shao, Qingyun Wu, and Huazheng Wang. Simpledoc: Multi-modal document understanding with dual-cue page retrieval and iterative refinement. In *Proceedings of the 2025 Conference on Empirical Methods in Natural Language Processing*, pages 28398–28415, 2025.
- Huiqiang Jiang, Qianhui Wu, Chin-Yew Lin, Yuqing Yang, and Lili Qiu. LLMingua: Compressing prompts for accelerated inference of large language models. In Houda Bouamor, Juan Pino, and Kalika Bali, editors, *Proceedings of the 2023 Conference on Empirical Methods in Natural Language Processing*, pages 13358–13376, Singapore, December 2023. Association for Computational Linguistics. doi: 10.18653/v1/2023.emnlp-main.825. URL <https://aclanthology.org/2023.emnlp-main.825/>.
- Bowen Jin, Hansi Zeng, Zhenrui Yue, Jinsung Yoon, Serkan Arik, Dong Wang, Hamed Zamani, and Jiawei Han. Search-r1: Training llms to reason and leverage search engines with reinforcement learning. *arXiv preprint arXiv:2503.09516*, 2025.
- Tom Kwiatkowski, Jennimaria Palomaki, Olivia Redfield, Michael Collins, Ankur Parikh, Chris Alberti, Danielle Epstein, Illia Polosukhin, Jacob Devlin, Kenton Lee, Kristina Toutanova, Llion Jones, Matthew Kelcey, Ming-Wei Chang, Andrew M. Dai, Jakob Uszkoreit, Quoc Le, and Slav Petrov. Natural questions: A benchmark for question answering research. *Transactions of the Association for Computational Linguistics*, 7:452–466, 2019. doi: 10.1162/tacl\_a\_00276. URL <https://aclanthology.org/Q19-1026/>.
- Woosuk Kwon, Zhuohan Li, Siyuan Zhuang, Ying Sheng, Lianmin Zheng, Cody Hao Yu, Joseph Gonzalez, Hao Zhang, and Ion Stoica. Efficient memory management for large language model serving with pagedattention. In *Proceedings of the 29th symposium on operating systems principles*, pages 611–626, 2023.
- Patrick Lewis, Ethan Perez, Aleksandra Piktus, Fabio Petroni, Vladimir Karpukhin, Naman Goyal, Heinrich Küttler, Mike Lewis, Wen-tau Yih, Tim Rocktäschel, et al. Retrieval-augmented generation for knowledge-intensive nlp tasks. *Advances in neural information processing systems*, 33:9459–9474, 2020.
- Jiawei Liu, Jia Le Tian, Vijay Daita, Yuxiang Wei, Yifeng Ding, Yuhan Katherine Wang, Jun Yang, and Lingming Zhang. Repoqa: Evaluating long context code understanding. *arXiv preprint arXiv:2406.06025*, 2024.
- Yubo Ma, Yuhang Zang, Liangyu Chen, Meiqi Chen, Yizhu Jiao, Xinze Li, Xinyuan Lu, Ziyu Liu, Yan Ma, Xiaoyi Dong, et al. Mmlongbench-doc: Benchmarking long-context document understanding with visualizations. *Advances in Neural Information Processing Systems*, 37:95963–96010, 2024.
- Zhuoshi Pan, Qianhui Wu, Huiqiang Jiang, Menglin Xia, Xufang Luo, Jue Zhang, Qingwei Lin, Victor Rühle, Yuqing Yang, Chin-Yew Lin, H. Vicky Zhao, Lili Qiu, and Dongmei Zhang. LLMingua-2: Data distillation for efficient and faithful task-agnostic prompt compression. In Lun-Wei Ku, Andre Martins, and Vivek Srikumar, editors, *Findings of the Association for Computational Linguistics: ACL 2024*, pages 963–981, Bangkok, Thailand, August 2024. Association for Computational Linguistics. doi: 10.18653/v1/2024.findings-acl.57. URL <https://aclanthology.org/2024.findings-acl.57/>.
- Qwen Team. Qwen3.5 technical report. <https://qwen.ai/blog?id=qwen3.5>, 2026.

- Phillip Rust, Jonas F Lotz, Emanuele Bugliarello, Elizabeth Salesky, Miryam de Lhoneux, and Desmond Elliott. Language modelling with pixels. *arXiv preprint arXiv:2207.06991*, 2022.
- Surya Prakash Sahu, Madhurima Mandal, Shikhar Bharadwaj, Aditya Kanade, Petros Maniatis, and Shirish Shevade. CodeQueries: A dataset of semantic queries over code. pages 1–11, 2024.
- Guangming Sheng, Chi Zhang, Zilingfeng Ye, Xibin Wu, Wang Zhang, Ru Zhang, Yanghua Peng, Haibin Lin, and Chuan Wu. Hybridflow: A flexible and efficient rlhf framework. *arXiv preprint arXiv: 2409.19256*, 2024.
- Zhaochen Su, Peng Xia, Hangyu Guo, Zhenhua Liu, Yan Ma, Xiaoye Qu, Jiaqi Liu, Yanshu Li, Kaide Zeng, Zhengyuan Yang, Linjie Li, Yu Cheng, Heng Ji, Junxian He, and Yi R. Fung. Thinking with images for multimodal reasoning: Foundations, methods, and future frontiers. *arXiv preprint arXiv:2506.23918*, 2025.
- Kaiser Sun, Xiaochuang Yuan, Hongjun Liu, Chen Zhao, Cheng Zhang, Mark Dredze, and Fan Bai. Reading, not thinking: Understanding and bridging the modality gap when text becomes pixels in multimodal llms. *arXiv preprint arXiv:2603.09095*, 2026.
- Yi Tay, Mostafa Dehghani, Dara Bahri, and Donald Metzler. Efficient transformers: A survey. *ACM Computing Surveys*, 55(6):1–28, 2022.
- Rahul Thapa, Kezhen Chen, Ian Covert, Rahul Chalamala, Ben Athiwaratkun, Shuaiwen Leon Song, and James Zou. Dragonfly: Multi-resolution zoom-in encoding enhances vision-language models. *arXiv preprint arXiv:2406.00977*, 2024.
- Rubèn Tito, Dimosthenis Karatzas, and Ernest Valveny. Hierarchical multimodal transformers for multipage docvqa. *Pattern Recognition*, 144:109834, 2023.
- Harsh Trivedi, Niranjan Balasubramanian, Tushar Khot, and Ashish Sabharwal. Musique: Multihop questions via single-hop question composition. *Transactions of the Association for Computational Linguistics*, 10:539–554, 2022.
- Ashish Vaswani, Noam Shazeer, Niki Parmar, Jakob Uszkoreit, Llion Jones, Aidan N Gomez, Łukasz Kaiser, and Illia Polosukhin. Attention is all you need. In I. Guyon, U. Von Luxburg, S. Bengio, H. Wallach, R. Fergus, S. Vishwanathan, and R. Garnett, editors, *Advances in Neural Information Processing Systems*, volume 30. Curran Associates, Inc., 2017. URL [https://proceedings.neurips.cc/paper\\_files/paper/2017/file/3f5ee243547dee91fbd053c1c4a845aa-Paper.pdf](https://proceedings.neurips.cc/paper_files/paper/2017/file/3f5ee243547dee91fbd053c1c4a845aa-Paper.pdf).
- Yibo Wang, Yongcheng Jing, Shunyu Liu, Hao Guan, Rong-cheng Tu, Chengyu Wang, Jun Huang, and Dacheng Tao. Vtc-r1: Vision-text compression for efficient long-context reasoning. *arXiv preprint arXiv:2601.22069*, 2026.
- Haoran Wei, Yaofeng Sun, and Yukun Li. DeepSeek-OCR: Contexts optical compression. *arXiv preprint arXiv:2510.18234*, 2025.
- Mingyuan Wu, Jingcheng Yang, Jize Jiang, Meitang Li, Kaizhuo Yan, Hanchao Yu, Minjia Zhang, Chengxiang Zhai, and Klara Nahrstedt. Vtool-r1: Vllms learn to think with images via reinforcement learning on multimodal tool use, 2025. URL <https://arxiv.org/abs/2505.19255>.
- Wenhao Wu, Yizhong Wang, Guangxuan Xiao, Hao Peng, and Yao Fu. Retrieval head mechanistically explains long-context factuality. *arXiv preprint arXiv:2404.15574*, 2024.
- Guangxuan Xiao, Yuandong Tian, Beidi Chen, Song Han, and Mike Lewis. Efficient streaming language models with attention sinks. *arXiv*, 2023.
- Roy Xie, Junlin Wang, Paul Rosu, Chunyuan Deng, Bolun Sun, Zihao Lin, and Bhuwan Dhingra. Knowing when to stop: Efficient context processing via latent sufficiency signals. *Advances in Neural Information Processing Systems*, 2025.
- Ling Xing, Alex Jinpeng Wang, Rui Yan, Xiangbo Shu, and Jinhui Tang. Vision-centric token compression in large language model. *arXiv preprint arXiv:2502.00791*, 2025.
- Zhilin Yang, Peng Qi, Saizheng Zhang, Yoshua Bengio, William Cohen, Ruslan Salakhutdinov, and Christopher D. Manning. HotpotQA: A dataset for diverse, explainable multi-hop question answering. In Ellen Riloff, David Chiang, Julia Hockenmaier, and Jun’ichi Tsujii, editors, *Proceedings of the 2018 Conference on Empirical Methods in Natural Language Processing*, pages 2369–2380, Brussels, Belgium, October–November 2018. Association for Computational Linguistics. doi: 10.18653/v1/D18-1259. URL <https://aclanthology.org/D18-1259/>.
- Howard Yen, Tianyu Gao, Minmin Hou, Ke Ding, Daniel Fleischer, Peter Izsak, Moshe Wasserblat, and Danqi Chen. Helmet: How to evaluate long-context language models effectively and thoroughly. In *International Conference on Learning Representations (ICLR)*, 2025.

Qiyong Yu, Zheng Zhang, Ruofei Zhu, Yufeng Yuan, Xiaochen Zuo, Yu Yue, Weinan Dai, Tiantian Fan, Gaohong Liu, Lingjun Liu, et al. Dapo: An open-source llm reinforcement learning system at scale. *arXiv preprint arXiv:2503.14476*, 2025.

Yaowei Zheng, Richong Zhang, Junhao Zhang, Yanhan Ye, Zheyang Luo, Zhangchi Feng, and Yongqiang Ma. Llamafactory: Unified efficient fine-tuning of 100+ language models. In *Proceedings of the 62nd Annual Meeting of the Association for Computational Linguistics (Volume 3: System Demonstrations)*, Bangkok, Thailand, 2024. Association for Computational Linguistics. URL <http://arxiv.org/abs/2403.13372>.

Ziwei Zheng, Michael Yang, Jack Hong, Chenxiao Zhao, Guohai Xu, Le Yang, Chao Shen, and Xing Yu. Deepeyes: Incentivizing "thinking with images" via reinforcement learning. *arXiv preprint arXiv:2505.14362*, 2025.

# Appendix

7	Implementation Details	15
7.1	Rendering	15
7.2	Training	16
7.3	Evaluation	16
7.4	Judge Model Agreement	16
8	Information-Theoretic Perspective	17
9	A Model-Agnostic Inference Framework	18
10	Efficiency Analysis and Limitations	19
11	Baseline and Compression Method Details	19
12	Dataset Statistics and Examples	20
12.1	Training and Evaluation Data	20
12.2	Hard Sample Filtering	21
13	Per-Dataset Results Across Compression Rates	21
14	Contamination-Free Evaluation	23
15	Ablation Analysis	23
15.1	SFT vs. RL Training	23
15.2	Oracle Image Selection	24
15.3	Effect of Multi-Turn Interaction	24
16	Generalization: Document and Code Understanding	25
16.1	Document Understanding	25
16.2	Code Understanding	25
17	Attention Analysis	26
17.1	Setup Details	26
17.2	Full Attention Shift After Training	26
18	Synthetic Trajectory Examples	27
19	Prompts	28

## 7 Implementation Details

### 7.1 Rendering

We render text into images using PIL with the DejaVuSans font (black text on a white background). Text is word-wrapped to fit the target image width. Each compression preset (Table 7) specifies the image width, font size, line spacing, margin, and tokens per image; these parameters fully determine how many characters fit per image, the image height, and thus the visual token count and compression rate. Because tokens per image differs across presets, a given document produces a *different* number of images at each preset (fewer, denser images at higher compression). Example renderings at each compression preset are shown in Figure 7.

**Vision encoder** The vision encoder (ViT) maps each image of resolution  $H \times W$  to

$$n = \frac{\lceil H/16 \rceil \times \lceil W/16 \rceil}{4} \quad (7.1)$$

visual tokens, where 16 is the grid stride and the division by 4 reflects  $2 \times 2$  spatial merging. The encoder operates at native resolution without any additional resizing.

We choose image widths that are multiples of 32 ( $= 16 \times 2$ ) so that  $\lceil W/16 \rceil$  and the merged output are exact integers with no rounding, making the visual token count deterministic. Image heights are controlled via the tokens-per-image parameter to also land on grid-aligned values. The resulting per-preset token counts are:  $5 \times$ :  $\lceil 284/16 \rceil \times \lceil 256/16 \rceil / 4 = 18 \times 16 / 4 = 72$ ;  $10 \times$ :  $\lceil 252/16 \rceil \times \lceil 192/16 \rceil / 4 = 16 \times 12 / 4 = 48$ ;  $15 \times$ :  $\lceil 190/16 \rceil \times \lceil 128/16 \rceil / 4 = 12 \times 8 / 4 = 24$ , yielding a clean 3:2:1 ratio across presets (Table 7).

This design means the compression rate is a product of two factors: higher text density per image (more characters packed into a smaller image) *and* fewer visual tokens per image (smaller images produce fewer patches). At  $5 \times$ , text is legible to the human eye; at  $10 \times$ , characters are small but distinguishable; at  $15 \times$ , most text is illegible. We train and evaluate on a mix of presets ( $5 \times$ ,  $10 \times$ ,  $15 \times$ ) unless otherwise noted.

For example, for a 10,000-token document, the three presets yield:  $5 \times$ :  $\lceil 10,000/405 \rceil = 25$  images  $\times$  72 VT = 1,800 VT ( $5.6 \times$  compression);  $10 \times$ : 19 images  $\times$  48 VT = 912 VT ( $11.0 \times$ );  $15 \times$ : 27 images  $\times$  24 VT = 648 VT ( $15.4 \times$ ). Image count stays in a narrow range (19–27) across presets; compression comes primarily from the per-image VT budget shrinking from 72 to 24 (a 3:1 ratio). The model sees a similar number of images at every compression rate, but each becomes smaller and less legible. Tokens per image is approximate and varies with actual content.

[Introduction]The history of computing is a fascinating journey that spans centuries of human ingenuity and innovation. From the earliest mechanical calculators to modern quantum computers, each era has brought transformative advances that reshaped how we process information, communicate, and understand the world around us. This document examines the key milestones, the brilliant minds behind them, and the societal impacts that followed. [Early Mechanical Devices] The abacus, dating back to approximately 2400 BCE in ancient Mesopotamia, represents one of humanity's first attempts to create a tool for calculation. While simple in design, consisting of beads on rods, it enabled merchants and administrators to perform arithmetic operations with remarkable speed and accuracy. Centuries later, in 1642, Blaise Pascal invented the Pascaline, a mechanical calculator capable of addition and subtraction. The device used a series of interlocking gears, with each gear representing a digit. When one gear completed a full rotation, it would advance the next gear by one position, implementing the carry operation mechanically. [Charles Babbage and Ada Lovelace] Charles Babbage is often called the father of computing for his conceptual designs of the Analytical Engine in the 1830s. Though never completed in his lifetime, this machine incorporated many features found in modern computers: an arithmetic logic unit, control flow through conditional branching and loops, and integrated memory. Ada Lovelace, working with Babbage, wrote what is widely considered the first computer program.

[Introduction]The history of computing is a fascinating journey that spans centuries of human ingenuity and innovation. From the earliest mechanical calculators to modern quantum computers, each era has brought transformative advances that reshaped how we process information, communicate, and understand the world around us. This document examines the key milestones, the brilliant minds behind them, and the societal impacts that followed. [Early Mechanical Devices] The abacus, dating back to approximately 2400 BCE in ancient Mesopotamia, represents one of humanity's first attempts to create a tool for calculation. While simple in design, consisting of beads on rods, it enabled merchants and administrators to perform arithmetic operations with remarkable speed and accuracy. Centuries later, in 1642, Blaise Pascal invented the Pascaline, a mechanical calculator capable of addition and subtraction. The device used a series of interlocking gears, with each gear representing a digit. When one gear completed a full rotation, it would advance the next gear by one position, implementing the carry operation mechanically. [Charles Babbage and Ada Lovelace] Charles Babbage is often called the father of computing for his conceptual designs of the Analytical Engine in the 1830s. Though never completed in his lifetime, this machine incorporated many features found in modern computers: an arithmetic logic unit, control flow through conditional branching and loops, and integrated memory. Ada Lovelace, working with Babbage, wrote what is widely considered the first computer program.

[Introduction]The history of computing is a fascinating journey that spans centuries of human ingenuity and innovation. From the earliest mechanical calculators to modern quantum computers, each era has brought transformative advances that reshaped how we process information, communicate, and understand the world around us. This document examines the key milestones, the brilliant minds behind them, and the societal impacts that followed. [Early Mechanical Devices] The abacus, dating back to approximately 2400 BCE in ancient Mesopotamia, represents one of humanity's first attempts to create a tool for calculation. While simple in design, consisting of beads on rods, it enabled merchants and administrators to perform arithmetic operations with remarkable speed and accuracy. Centuries later, in 1642, Blaise Pascal invented the Pascaline, a mechanical calculator capable of addition and subtraction. The device used a series of interlocking gears, with each gear representing a digit. When one gear completed a full rotation, it would advance the next gear by one position, implementing the carry operation mechanically. [Charles Babbage and Ada Lovelace] Charles Babbage is often called the father of computing for his conceptual designs of the Analytical Engine in the 1830s. Though never completed in his lifetime, this machine incorporated many features found in modern computers: an arithmetic logic unit, control flow through conditional branching and loops, and integrated memory. Ada Lovelace, working with Babbage, wrote what is widely considered the first computer program.

(a)  $5 \times$  compression

(b)  $10 \times$  compression

(c)  $15 \times$  compression

**Figure 7** The same source text rendered at three compression presets. At  $5 \times$ , text is legible to the human eye. At  $10 \times$  and  $15 \times$ , characters become progressively illegible. The visual token count decreases with compression, where the compression rate reflects both higher text density and fewer visual tokens per image.

**Table 7** Rendering presets. Higher compression packs more text into fewer visual tokens per image, yielding a 3:2:1 VT ratio across presets. Image widths are multiples of 32 for grid-aligned vision-encoder tokenization.

Preset	Width (px)	Font (pt)	Line sp.	Margin (px)	Tok/img	Height (px)	VT/img	~Chars/img
5×	256	8	1.15	7	405	284	72	2,000
10×	192	6	1.10	6	540	252	48	2,700
15×	128	5	1.05	5	378	190	24	1,900

## 7.2 Training

During both SFT and RL, we freeze the vision encoder and visual projector and only update the language model parameters. Recent work (Sun et al., 2026) shows that adapting the language model is sufficient for text-visual compression reading task, while training the vision encoder yields no additional benefit. This also reduces memory and compute cost, as gradients need not flow through the vision encoder. All training and evaluation are done using 8× B200 GPUs.

For SFT, we finetune Qwen3.5-9B-Base using LLaMA-Factory (Zheng et al., 2024) with DeepSpeed ZeRO-3 (Aminabadi et al., 2022), learning rate  $5 \times 10^{-6}$ , effective batch size 64 (batch size 2 per GPU with gradient accumulation 4) for 2 epochs on the hard subset. Training data is formatted in ShareGPT multi-turn conversation format with interleaved image tokens.

For RL, we use VERL (Sheng et al., 2024) to run DAPO (Yu et al., 2025) starting from the SFT checkpoint on 15K samples subsampled from the remaining hard samples and easy samples, with learning rate  $10^{-7}$ , batch size 32, 16 rollouts per prompt, temperature 0.8, up to 6 tool calls per episode, and no entropy regularization. Our scaling experiments in Section 5.4 are limited to 9B parameters due to compute budget. Our generic inference framework and post-training recipe should generalize to larger models, we leave this to future work.

We use Qwen3.5-9B-Base (Qwen Team, 2026) as our backbone VLM. It couples a 9B-parameter language decoder with a vision encoder (ViT with spatial merging) that maps each image into a resolution-dependent number of visual tokens (Table 7 in Section 7.1). We select Qwen3.5-9B for three reasons: (1) it natively supports interleaved image-text inputs, which is required for our multi-turn tool-use format; (2) its vision encoder handles variable-resolution images without resizing, preserving rendered-text fidelity; and (3) scaling experiments (§5.4) show that 9B is the minimum scale at which reliable tool-use behavior emerges.

## 7.3 Evaluation

We serve all models for evaluation using vLLM (Kwon et al., 2023). Models are allowed up to 6 turns with greedy decoding (temperature 0.0) and max response tokens of 2,048 per turn. At each turn, the model may invoke the EXPAND tool; the tool response is appended to the conversation and the model continues until it produces a final answer or exhausts the turn budget. The LLM judge (§4.1) is hosted separately via vLLM and scores each response with greedy decoding.

**Table 8** Judge model agreement. Qwen3.5-397B and GPT-oss 120B differ by only 0.3 pp overall ( $\kappa = 0.81$ ), confirming that our conclusions are judge-independent.

Compression	Qwen3.5-397B Acc.	GPT-oss 120B Acc.	$\Delta$	Agreement	Cohen’s $\kappa$
5×	68.9	68.1	−0.8	92.7%	0.81
10×	62.1	62.8	+0.7	91.5%	0.80
15×	52.1	51.2	−0.9	90.8%	0.81
<b>Overall</b>	61.0	60.7	−0.3	91.7%	0.81

## 7.4 Judge Model Agreement

We evaluate two judges’ agreement on our main text QA results: GPT-oss 120B (Agarwal et al., 2025) and Qwen3.5-397B. Both judges use identical prompts (Section 19) and greedy decoding on the same (question,

gold answer, model prediction) triples across all three compression rates. The two judges differ by only 0.3 pp overall with inter-judge agreement of 91.7% (Table 8).

## 8 Information-Theoretic Perspective

We discuss the design motivation behind LensVLM from an information-theoretic perspective.

**Information can be lost at rendering and at encoding.** Rendering maps text  $\mathcal{D} = (t_1, \dots, t_N)$  into images  $\mathcal{V} = f(\mathcal{D})$  through a deterministic renderer  $f$ , and the model observes visual tokens  $\mathcal{T} = g(\mathcal{V})$  via the vision encoder  $g$ . Determinism does not imply injectivity: at sufficiently aggressive compression, two different strings can render to indistinguishable pixel images (e.g., Figure 7(c) in Section 7.1). Applying the data processing inequality through both stages,

$$I(a^*; \mathcal{T} | q) \leq I(a^*; \mathcal{V} | q) \leq I(a^*; \mathcal{D} | q), \quad (8.1)$$

so failures under compression can arise either because the renderer destroys answer-relevant information or because the vision encoder cannot recover it. The EXPAND tool does not introduce information beyond the source: the returned content  $\tau_k$  is a deterministic function of  $\mathcal{D}$ . Its role is representational; it presents a selected region in a form that is easier for the model to read (source text or a high-resolution image) rather than asking the model to extract all fine-grained content from compressed visual tokens.

**Selection and extraction have different targets.** Image selection and answer extraction ask the model to predict different variables: selection identifies an evidence set  $E^* \subseteq \{1, \dots, K\}$  (a single image for single-hop queries, multiple for multi-hop), while extraction predicts an answer string  $a^*$  over a much larger, content-dependent space. This asymmetry suggests (but does not prove) that compressed visual tokens may preserve enough coarse cues for selection even when they do not support reliable character-level reading. Whether this holds is a property of the task distribution and model rather than a theorem: in corner cases such as a factoid whose only clue is a short phrase on one image, selecting the correct image may require reading nearly the same text needed to answer the question.

**When selective expansion helps.** The preceding points suggest when selective expansion should help. Let  $\bar{D}(\pi)$  denote the expected task error under policy  $\pi$ , marginalizing over all subsets  $S \subseteq \{1, \dots, K\}$  that  $\pi$  may select for expansion. Conditioning on whether all evidence images are included,

$$\bar{D}(\pi) = p_\pi D_{\text{hit}} + (1 - p_\pi) D_{\text{miss}}, \quad (8.2)$$

where  $p_\pi = P_\pi(E^* \subseteq S)$ ,  $D_{\text{hit}}$  is the expected error when all evidence images are expanded, and  $D_{\text{miss}}$  is the error when at least one is not (for multi-hop queries with  $|E^*| > 1$ , this averages over partial-retrieval cases). Let  $D_{\text{no}}(\rho)$  be the error of answering directly from compressed images at compression rate  $\rho$ . The benefit of selective expansion is

$$D_{\text{no}}(\rho) - \bar{D}(\pi) = p_\pi (D_{\text{no}}(\rho) - D_{\text{hit}}) - (1 - p_\pi) (D_{\text{miss}} - D_{\text{no}}(\rho)). \quad (8.3)$$

This makes the tradeoff explicit: tool use helps when the gain from correctly expanding all evidence images outweighs the penalty from missing evidence or being misled by expanded distractors. The decomposition is exact but does not require  $D_{\text{hit}}$  to match the full-text error or  $D_{\text{miss}}$  to match the no-tool compressed-image error; expanding the wrong images can hurt if the model over-focuses on irrelevant tool responses.

The perspective predicts a useful compression regime: tool use helps when direct reading degrades faster than selection accuracy. Our main results confirm LensVLM operates in this regime across all studied compression rates (Figure 3 in §4.2), with the advantage growing as compression increases. The pattern is model-dependent: the untrained base model’s selection degrades much faster (Section 8), and attention shifts increasingly toward tool-response tokens at higher compression (§5.2).

**Empirical verification.** We evaluate whether the untrained base model can use compressed images for evidence localization by comparing QA and selection accuracy across compression rates on the standard multi-preset test set (Section 12).

For QA accuracy, the base model receives all compressed images and answers the question directly. For selection accuracy, it receives the same images but is instead prompted to identify which image contains the answer. Both tasks use greedy decoding. QA is scored by the LLM judge, while selection is scored by whether the predicted image matches any ground-truth evidence image. For multi-hop queries (MuSiQue, 2 – 4 evidence images), this “any-hit” criterion is deliberately lenient; QA accuracy remains the primary metric because answering correctly requires retrieving evidence across multiple EXPAND calls. Table 13 (Section 15.1) shows that, without training, the base model’s direct QA accuracy falls from 31.3% at 5× to 18.1% at 15× (42% relative drop). Selection accuracy is substantially lower: the untrained model reaches only 25.8% at 5× and drops to 18.0% at 10× (30% relative degradation, over the same range where QA drops 33%), indicating that the base model cannot reliably localize evidence from compressed images.

These results show that the information-theoretic argument is not sufficient on its own. Although selection is a plausible lower-dimensional target than extraction, the pretrained model does not already know how to use compressed images for localization. Post-training changes this behavior substantially: after SFT+RL, selection accuracy reaches 76.8%/71.0%/52.1% at 5×/10×/15× (Table 13 in Section 15.1). Thus, selection from compressed images is learnable, but it is not guaranteed by information-theoretic considerations alone.

## 9 A Model-Agnostic Inference Framework

The selection-then-expansion framework (scan compressed images, identify the relevant image, expand to uncompressed form) is not tied to a particular model. To quantify the framework’s standalone value, we apply it to two model families without any task-specific training: (1) an open-weight 9B VLM (Qwen3.5-9B-Base) and (2) a frontier model (Sonnet 4.6 (Anthropic, 2026)). In both cases, the model receives compressed images, predicts which image contains the answer, and then receives that image’s content as uncompressed text before generating its final answer.

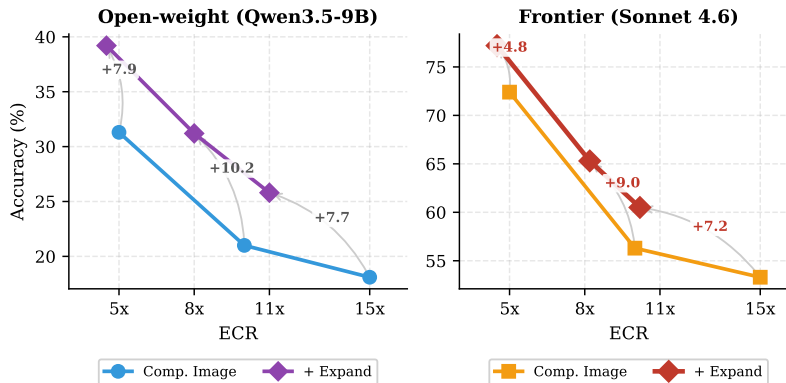


**Figure 8** The EXPAND tool improves accuracy for both open-weight (9B) and frontier (Sonnet 4.6) models at every compression level without any fine-tuning.

**The tool provides consistent gains across model families.** Figure 8 shows that selecting and expanding improves accuracy for both model families at every compression level, with no training required. The untrained 9B model gains +7.9 to +10.2 pp; Sonnet 4.6 gains +4.8 to +9.0 pp on average. These results confirm that the bottleneck we address (information loss from visual compression) affects models regardless of scale, and the select-then-expand framework is a general-purpose inference strategy.

## 10 Efficiency Analysis and Limitations

We profile inference efficiency on Qwen3.5-9B (8 full-attention layers, 4 KV heads, head\_dim 256, bf16), which costs 32 KiB of KV cache per token per GPU. At 15× compression with 20 input images, the Text baseline consumes 10,686 prompt tokens (334 MiB KV), while LensVLM consumes 2,288 tokens after all EXPAND calls (71 MiB KV), a 78.6% reduction. At 100 images, Text requires 51,273 tokens (1,602 MiB) versus LensVLM’s 8,090 tokens (253 MiB), an 84.2% reduction. These token counts are the peak KV cache occupancy at the final inference turn (measured via vLLM, TP=8, B200 GPUs); because the KV cache grows monotonically across turns, the final turn is the peak.

The primary cost is latency: with one EXPAND call (the typical case), LensVLM requires two sequential inference turns totaling  $\sim 17$ s compared to  $\sim 8$ s for the single-turn Text baseline ( $\sim 2\times$  overhead, measured at batch size 1 with 256 generation tokens on B200). This overhead has two sources: (1) multi-turn sequential decoding, where each EXPAND forces a generate-then-prefill round-trip that cannot be parallelized, and (2) vision encoder processing, since each rendered image must pass through the ViT encoder and projector before entering the language model, an overhead that text-only baselines bypass entirely. Both are inherent to the current VLM tool-use architecture rather than specific to our method: any system that augments generation with tool calls pays the same multi-turn tax. LensVLM targets accuracy recovery under lossy visual compression, not inference speed; reducing this overhead via parallel tool dispatch or cached vision encodings is an engineering direction we leave to future work. A secondary cost is storage: the EXPAND tool requires access to source text (or original images for the zoom variant), but this is negligible relative to the VRAM savings (GPU memory is roughly  $200\times$  more expensive per GB than SSD at typical cloud pricing).

## 11 Baseline and Compression Method Details

Long-context compression can be approached through text-space methods or visual compression, but each has structural limitations. In text space, token-pruning methods (Jiang et al., 2023; Pan et al., 2024) irreversibly discard tokens with no recovery path. Tokenizer-based approaches require an expanded vocabulary and model retraining for each target compression rate, since the rate is baked into the vocabulary. In contrast, visual tokenization requires no vocabulary changes: VLMs already process images natively, so the compression rate is controlled simply by adjusting the rendered image size. Visual compression methods like Glyph (Cheng et al., 2025) improve reading from compressed renderings, but still rely on a fixed compressed view with no mechanism to recover information lost to the vision encoder; this helps at lower compression rates but inevitably hits a ceiling at higher compression.

**Effective Compression Rate Computation** We report both ICR ( $C_{\text{in}}$ , Equation (3.1)) and ECR ( $C_{\text{eff}}$ , Equation (3.3)) in this work. Every baseline family process input images through a different mechanism, producing different achieved ECR. As noted in §3.3, retrieval is not compression in the LensVLM sense (the full context is processed at index time); we report ECR based on per-query reader input for fair comparison.

- **Text-retrieval** (BM25, BGE-M3, Jina-Text, Qwen3-Emb): Documents are split into chunks matching the text capacity of one rendered image at the corresponding preset. The retriever returns the top  $\lceil K/C_{\text{in}} \rceil$  chunks; ECR counts only the retrieved text tokens passed to the reader.
- **Image-retrieval** (ColPali, Jina-Multimodal): The retriever scores rendered images and returns the top  $\lceil K/C_{\text{in}} \rceil$ ; the reader receives the text contained in those images. ECR counts the returned reader text, not the images consumed by the retriever.
- **Text-compression** (LLMLingua-2): Uses a soft target ICR as a parameter, but because token-level pruning is based on perplexity, the achieved ECR varies by task and can exceed the target.
- **Compressed-image** (Image, Glyph, hybrids): Compression is fixed by rendering preset. For Glyph, the ECR differs because GLM-4.1V produces more visual tokens per image (Section 11); achieved ECR is  $4.5\times/8.6\times/10.8\times$  at the  $5\times/10\times/15\times$  presets.

- **Reference baselines:** *Text* feeds the full document ( $C_{\text{in}}=1$ ). *Oracle Images* feeds only gold-evidence text ( $C_{\text{in}} \approx 15\times$ ) but presupposes oracle access and is a non-achievable upper bound.
- **LensVLM:** ICR is the rendering preset; ECR is lower because EXPAND calls append tokens, but adaptive across queries (easy queries retain  $C_{\text{eff}} = C_{\text{in}}$ ).

**Model-based visual compression.** When a model-based baseline uses a different vision encoder, its ECR differs from the nominal ICR. Our presets are designed for Qwen3.5’s encoder (Equation (7.1)), which produces  $n = \lceil H/16 \rceil \times \lceil W/16 \rceil / 4$  tokens per image. Glyph uses GLM-4.1V-9B-Base, whose encoder has patch size 14 and spatial merge size 2, yielding

$$n_{\text{GLM}} = \text{round}(H/28) \times \text{round}(W/28) \tag{11.1}$$

tokens per image. This produces 25–46% more visual tokens than Qwen3.5 at our preset dimensions:

Preset	Image (W×H)	Qwen3.5 VT	GLM-4.1V VT	Qwen3.5 ECR	Glyph ECR
5×	256×284	72	90	5.0×	4.5×
10×	192×252	48	63	10.0×	8.6×
15×	128×190	24	35	15.0×	10.8×

The discrepancy arises because Qwen3.5 uses patch stride 16 with 2×2 merge (effective 32×32 px/token) while GLM-4.1V uses patch size 14 with 2×2 merge (effective 28×28 px/token). We report Glyph’s achieved ECR in Table 11 (Section 13); in general, any model-based baseline should report ECR from its own encoder’s tokenization formula.

## 12 Dataset Statistics and Examples

### 12.1 Training and Evaluation Data

We use four following datasets for training:

- **NQ** (Kwiatkowski et al., 2019): Single-hop factoid questions from Google search queries paired with Wikipedia articles. Answers are short spans (named entities, dates, quantities).
- **HotpotQA** (Yang et al., 2018): Multi-hop questions requiring composition of 2 supporting facts from Wikipedia.
- **MuSiQue** (Trivedi et al., 2022): Multi-hop questions requiring 2–4 reasoning steps, harder than HotpotQA due to longer chains.
- **HELMET** (Yen et al., 2025): Diverse QA tasks over naturally long documents (up to 32K tokens).

Following §3.4, documents are padded with distractor text to 3K–32K tokens and rendered at three presets (5×, 10×, 15×). Each sample is assigned a single preset; the three are balanced in the final mixture. Table 9 summarizes the corpus. From 143,145 generated samples with successful distillation traces, approximately 105,000 are retained as hard after filtering (Section 12.2). We allocate 80% of hard samples for SFT and subsample from the remaining 20% combined with easy samples for RL. The in-domain (ID) test set contains 2,400 samples (4 datasets × 3 presets × 200). The out-of-domain (OOD) test set contains 1,711 unique samples rendered at all three presets (5,133 total evaluations).

**Table 9** Training data composition. All four datasets average  $\sim 25$  images and  $\sim 10\text{K}$  tokens per sample; 73.5% of samples are classified as hard.

Dataset	Generated	Hard	Test	Hops	Avg. tokens	Avg. images
NQ	36,600	28,877	600	1	9,800	25
HotpotQA	89,364	61,482	600	2	10,200	25
MuSiQue	14,503	12,920	600	2-4	9,600	25
HELMET	2,678	1,923	600	1	10,500	26
<b>Total</b>	<b>143,145</b>	<b>105,202</b>	<b>2,400</b>	–	9,800	25

The OOD set spans 14 datasets from three suites: RULER (Hsieh et al., 2024) (QA subsets; original 128K contexts truncated to  $\sim 32\text{K}$  tokens by removing padding while preserving needle evidence), Qasper (Dasigi et al., 2021), and LongBench (Bai et al., 2024) (12 subtask variants covering multi-hop QA, passage retrieval, summarization, and single-document QA). Per-benchmark results in Table 11 (Section 13).

## 12.2 Hard Sample Filtering

The filtering (§3.4) follows three steps:

1. **Base model inference.** Base model served via vLLM runs single-turn inference on all training samples. The model sees rendered images and the question, producing a direct answer.
2. **Judging.** Each prediction is evaluated via a LLM judge.
3. **Filtering.** Correctly answered samples are discarded. 80% of hard samples go to SFT; the remaining 20% are combined with easy samples for RL.

Table 10 reports per-dataset filtering rates. Keep rate varies substantially: MuSiQue retains 89.1% (base accuracy 10.9%) while HotpotQA retains 68.8% (base accuracy 31.2%).

**Table 10** Hard sample filtering statistics. Multi-hop reasoning is the primary difficulty.

Dataset	Source	Kept (hard)	Keep rate	Base acc.
MuSiQue	14,503	12,920	89.1%	10.9%
NQ	36,600	28,877	78.9%	21.1%
HELMET	2,678	1,923	71.8%	28.2%
HotpotQA	89,364	61,482	68.8%	31.2%
<b>Total</b>	<b>143,145</b>	<b>105,202</b>	<b>73.5%</b>	<b>26.5%</b>

## 13 Per-Dataset Results Across Compression Rates

Table 11 reports per-dataset QA accuracy for all baselines at  $5\times$ ,  $10\times$ , and  $15\times$  compression; Table 12 reports the corresponding selection accuracy for LensVLM variants. Text retrieval selects  $k = \lceil K/C_{\text{in}} \rceil$  images at each target rate; prompt compression retains the corresponding fraction of tokens. Image methods use the matching rendering preset. All results are averaged over three runs.

**Table 11** Full per-dataset results on text QA. LensVLM achieves the highest or tied-highest average accuracy at every compression rate in average.

Method			In-Domain				Out-of-Domain			Avg.
	ICR	ECR	NQ	HotpotQA	MuSiQue	HELMET	RULER	Qasper	LongBench	
Text	1×	1.0×	80.8	86.7	68.7	76.2	70.7	61.3	62.5	72.4
<i>Upper bounds</i>										
<i>5× compression</i>										
Comp. Image	5×	5×	42.5	33.5	19.5	33.1	35.6	25.3	29.8	31.3
Glyph	5×	4.5×	57.5	42.0	33.0	63.5	64.9	31.9	37.9	47.2
LLMLingua-2	5×	5.5×	62.2	47.5	33.8	58.7	56.1	33.5	38.3	47.2
Base + Expand	5×	4.5×	55.5	45.5	34.0	35.0	38.5	37.9	28.2	39.2
BM25	5×	4.5×	73.0	80.0	53.2	70.3	67.4	42.7	50.6	62.5
BGE-M3	5×	4.5×	76.5	80.0	59.0	73.8	67.0	45.8	53.8	65.1
Jina-v4	5×	4.5×	74.8	80.7	57.5	73.7	66.9	50.9	49.5	64.9
Qwen3-Emb	5×	4.5×	73.7	77.8	56.5	72.7	66.9	52.2	51.3	64.4
ColPali	5×	4.7×	64.5	70.0	49.5	71.5	56.6	35.8	44.6	56.1
Jina-v4-MM	5×	4.6×	69.5	79.0	58.5	73.0	68.4	47.3	49.9	63.7
LensVLM <sub>SFT</sub>	5×	4.6×	68.4	80.3	66.1	72.7	60.7	43.3	54.1	63.7
LensVLM	5×	4.3×	76.1	81.5	69.6	78.4	65.5	48.3	62.6	68.9
<i>10× compression</i>										
Comp. Image	10×	10×	33.0	29.0	14.0	22.5	21.3	8.8	18.7	21.0
Glyph	10×	8.6×	47.5	37.5	26.5	50.5	58.6	12.1	21.9	36.4
LLMLingua-2	10×	11.3×	55.0	39.2	26.5	50.8	42.0	24.5	25.5	37.6
Base + Expand	10×	8.0×	52.5	40.0	15.0	30.5	30.5	25.3	24.8	31.2
BM25	10×	8.3×	66.8	71.5	43.8	65.5	65.7	33.9	42.8	55.7
BGE-M3	10×	8.3×	72.2	67.8	48.0	68.3	63.4	34.6	45.6	57.1
Jina-v4	10×	8.3×	70.0	73.0	47.7	69.7	65.3	36.1	43.2	57.9
Qwen3-Emb	10×	8.3×	69.3	68.3	48.2	70.0	60.3	36.3	42.9	56.5
ColPali	10×	8.3×	63.0	56.0	32.5	60.0	48.3	31.9	34.4	46.6
Jina-v4-MM	10×	8.3×	72.0	73.5	45.0	63.0	51.1	39.0	38.8	54.6
LensVLM <sub>SFT</sub>	10×	8.1×	67.9	72.2	59.9	63.2	55.1	36.0	44.0	56.9
LensVLM	10×	7.4×	75.1	75.5	62.4	71.5	60.8	38.5	50.9	62.1
<i>15× compression</i>										
Comp. Image	15×	15×	34.0	25.0	12.5	24.5	16.1	2.8	11.9	18.1
Glyph	15×	10.8×	50.0	31.5	21.0	46.0	54.8	7.7	18.4	32.8
LLMLingua-2	15×	15.7×	49.2	36.8	21.8	47.2	36.2	16.8	23.3	33.0
Base + Expand	15×	11.0×	49.0	32.0	12.5	24.5	25.3	15.4	21.7	25.8
BM25	15×	11.9×	65.8	65.0	36.8	63.5	54.5	30.4	39.8	50.8
BGE-M3	15×	11.9×	69.7	62.0	40.2	67.8	51.3	31.1	41.1	51.9
Jina-v4	15×	11.9×	67.2	63.2	41.7	68.8	53.6	31.0	39.1	52.1
Qwen3-Emb	15×	11.9×	66.0	62.3	41.3	67.5	49.8	33.2	37.9	51.1
ColPali	15×	11.9×	58.0	50.0	31.5	57.0	39.7	21.4	35.7	41.9
Jina-v4-MM	15×	11.9×	71.0	56.5	39.0	69.0	46.6	33.5	36.3	50.3
LensVLM <sub>SFT</sub>	15×	10.7×	61.6	60.6	41.2	51.7	48.1	24.4	32.5	45.7
LensVLM	15×	10.1×	71.2	64.5	49.0	57.2	52.7	28.4	42.0	52.1

**Table 12** Per-dataset selection accuracy. RL consistently improves over SFT, with the largest gains at 10× (+6.3 pp avg.) and 15× (+6.2 pp avg.) where visual information is most degraded.

Method	ICR	In-Domain				Out-of-Domain			Avg.
		NQ	HotpotQA	MuSiQue	HELMET	RULER	Qasper	LongBench	
<i>5× compression</i>									
LensVLM <sub>SFT</sub>	5×	78.5	82.2	76.0	74.8	73.7	66.3	76.3	75.4
LensVLM	5×	80.7	82.4	79.2	76.3	74.0	67.1	77.9	76.8
<i>10× compression</i>									
LensVLM <sub>SFT</sub>	10×	73.0	76.8	69.4	64.1	60.5	51.7	57.4	64.7
LensVLM	10×	79.2	83.0	76.5	70.3	66.1	58.0	63.9	71.0
<i>15× compression</i>									
LensVLM <sub>SFT</sub>	15×	61.0	55.8	40.6	49.7	44.8	26.2	43.2	45.9
LensVLM	15×	71.4	65.8	50.2	59.0	47.3	32.1	38.9	52.1

## 14 Contamination-Free Evaluation

We fetch 55,872 PubMed Central open-access articles, restricted to publications between February 16 and April 1, 2026 (after Qwen3.5’s pre-training cutoff). For each article, Qwen3.5-397B generates a single-hop QA pair conditioned on a unique document chunk (one QA per chunk, no chunk reuse). After question quality filtering, the final corpus contains 26,164 training samples and 533 held-out test samples. Each sample is rendered using the same rendering pipeline. The training procedure follows §3.5.

## 15 Ablation Analysis

### 15.1 SFT vs. RL Training

Table 13 isolates the contribution of each training stage. SFT teaches the complete tool-use pipeline: format, selection, and extraction simultaneously, reaching 75%/65%/46% selection accuracy at 5×/10×/15×. RL does not introduce new capabilities but refines the model’s judgment about *where* to apply them. Because SFT trains on teacher-generated trajectories, the model inherits the teacher’s image-selection distribution rather than learning from its own mistakes. On-policy RL closes this gap: selection accuracy improves most at higher compression where the overview is least legible and selection is hardest (+6.3 pp at 10×, +6.2 pp at 15×), indicating that RL teaches the model to extract subtler cues from degraded compressed images. RL also improves reasoning over expanded content, adding +5–6 pp QA accuracy consistently across all compression rates.

**Table 13** Training stage ablation. SFT teaches the tool-use format (+32 pp at 5×); RL adds +5–6 pp QA and further improves selection, especially at higher compression.

Model	QA Accuracy			Selection Accuracy		
	5×	10×	15×	5×	10×	15×
Base	31.3	21.0	18.1	25.8	18.0	18.3
+ SFT	63.7	56.9	45.7	75.4	64.7	45.9
+ SFT + RL (LensVLM)	<b>68.9</b>	<b>62.1</b>	<b>52.1</b>	<b>76.8</b>	<b>71.0</b>	<b>52.1</b>

RL does increase the EXPAND call rate relative to SFT, lowering ECR from 4.6×/8.1×/10.7× to 4.3×/7.4×/10.1× at 5×/10×/15× (Table 11 in Section 13). This is a side effect of the tool-use bonus in the reward; however, the additional calls co-occur with improved QA accuracy (+5.2/+5.2/+6.4 pp) and selection accuracy (+1.4/+6.3/+6.2 pp), indicating that the extra expansions are productive rather than degenerate.

## 15.2 Oracle Image Selection

To disentangle LensVLM’s gains from learned image selection versus the end-to-end tool-use format, we evaluate ablation baselines that isolate the selection component (Table 14). This analysis is focused on the in-domain test set where ground-truth evidence image labels are available. *Oracle Selection* bypasses the model’s selection and feeds GT evidence texts directly, providing a ceiling. *Img + Oracle Text* feeds all compressed images together with GT text. *Base + Expand* uses the untrained base model to predict the evidence image, isolating how much of LensVLM’s advantage comes from trained selection versus the tool-use protocol itself.

**Table 14** Oracle selection analysis (in-domain, 4 datasets  $\times$  200 samples/preset). LensVLM (76.4% at 5 $\times$ ) approaches the oracle ceiling (80.0%), while untrained Base + Expand (42.5%) confirms that post-training is essential for effective selection.

Method	5 $\times$	10 $\times$	15 $\times$
Comp. Image (no tool)	32.1	24.6	24.0
Base + Expand	42.5	34.5	29.5
LensVLM	76.4	71.1	60.5
Img + Oracle Text	67.4	79.1	74.4
Oracle Selection (text)	80.0	80.0	80.0
Text (upper bound)	78.1	78.1	78.1

Oracle Selection (80.0%) exceeds the in-domain Text upper bound (78.1%, computed on the same 4 datasets) because the reader receives only the concise GT image text rather than the full document, reducing noise. LensVLM (76.4% at 5 $\times$ ) approaches this ceiling despite learning selection from compressed images. The Base + Expand baseline (42.5%) confirms that untrained selection is far weaker and post-training is essential. Img+Oracle Text shows a compression-dependent interaction: at 5 $\times$ , many high-resolution images hurt reading (67.4% vs. 78.1% text) as the model attends to visual noise; at 10 $\times$ + the less informative compressed images cause less distraction and performance matches the text baseline.

## 15.3 Effect of Multi-Turn Interaction

Our method allows the model to call EXPAND multiple times per query. We ablate the effect of the tool-call budget by running inference once with a generous limit (7 calls) and retroactively evaluating accuracy at each budget  $m \in \{1, \dots, 7\}$ : for trajectories that used more than  $m$  calls, we force-extract the answer from the response at call  $m$ .

Figure 9 shows that a single EXPAND call provides most of the signal: accuracy reaches 60.8% after just one call, confirming the effectiveness of enabling tool-use. A second call adds +6.1 pp (66.9%), capturing multi-hop queries that require a second piece of evidence. Returns diminish rapidly after 2 calls: +1.6 (3 calls), +1.1 (4 calls), and <0.5 thereafter. In practice, the average trajectory uses only 1.3 EXPAND calls and nearly all trajectories complete within 5 calls, justifying the default budget of 5 calls ( $T=6$  turns). MuSiQue benefits most from additional calls, gaining +22 pp between 1 and 4 calls (40.3% $\rightarrow$ 62.5%) compared to +3.4 for HELMET and +8.2 for HotpotQA, consistent with its multi-hop evidence requirements.

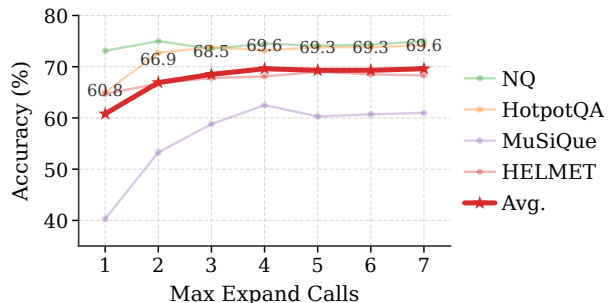


**Figure 9** Effect of EXPAND budget on QA accuracy. One call captures most of the gain (60.8%); the model self-regulates to  $\sim$ 1.3 calls even with generous budgets.

## 16 Generalization: Document and Code Understanding

We evaluate LensVLM on two transfer domains beyond rendered text QA.

### 16.1 Document Understanding

MMLongBench-Doc contains long PDF documents (up to 200 images) spanning reports, academic papers, and administrative forms. Document images are natively rendered (not text rendered to images as in our main pipeline). Compressed thumbnails are created by downscaling each image’s pixel count by  $N\times$ : the scale per spatial dimension is  $1/\sqrt{N}$ , so a typical 150-DPI image ( $\sim 1275\times 1650$ ,  $\sim 2.1\text{M}$  pixels) becomes  $\sim 570\times 737$  at  $5\times$ ,  $\sim 403\times 521$  at  $10\times$ , and  $\sim 329\times 426$  at  $15\times$ .

Training data comes from MP-DocVQA (Tito et al., 2023) and DocVQA: 10,256 raw samples filtered for OCR answer recall (the gold answer must appear in at least one image’s OCR text), balanced across presets ( $\sim 3,300$  each). Synthetic tool use and reasoning traces are generated via the same pipeline as in the main experiment. Two tool variants are trained: (1) **OCR text**: `read_image` returns PaddleOCR-VL text from the full-resolution image; (2) **Image zoom**: `read_image` returns the full-resolution image directly. Both use identical training procedure. We set `image_min_pixels=1` to prevent upsampling of compressed thumbnails and `image_max_pixels=4,194,304` (4M) to accommodate full-resolution images returned by the zoom tool.

**OCR engine selection.** We evaluated PaddleOCR-VL (Cui et al., 2026) and DeepSeekOCR-v2 (Wei et al., 2025) and found that PaddleOCR-VL produces consistent extraction quality across our rendering configurations, whereas DeepSeekOCR-v2 exhibited higher variance on narrow or heavily compressed renders. Therefore, we use PaddleOCR-VL for the OCR text tool in this work.

### 16.2 Code Understanding

We evaluate on two code benchmarks: RepoQA (Liu et al., 2024), a function retrieval task over long code repositories from 6 programming languages, and CodeQueries (Sahu et al., 2024), a semantic query task over Python code. The total number of code samples is 917. Code is rendered into images using the same PIL-based pipeline as text (§3.1). Table 15 breaks down the aggregate code results by dataset.

**Table 15** Per-dataset code results. RepoQA drives aggregate performance; LensVLM’s advantage over Glyph widens at higher compression.

Dataset	Method	5×	10×	15×
RepoQA	Text	92.4	92.4	92.4
	Comp. Image	43.0	11.6	6.4
	Glyph	55.2	17.4	12.8
	LensVLM	<b>63.4</b>	<b>40.7</b>	<b>29.7</b>
CodeQueries	Text	38.7	38.7	38.7
	Comp. Image	10.3	0.5	0.0
	Glyph	8.3	1.9	1.2
	LensVLM	<b>12.8</b>	<b>11.5</b>	<b>10.3</b>

RepoQA is the primary driver of aggregate performance: LensVLM maintains 63.4% at  $5\times$  (vs. 92.4% text upper bound), and the gap to Image and Glyph widens at higher compression (+20 pp and +17 pp over Glyph at  $10\times$  and  $15\times$ ). CodeQueries is substantially harder for all methods; the text upper bound is only 38.7%, and compressed-image baselines collapse to near-zero at  $10\times$  and above. LensVLM maintains 10–13% across all presets on CodeQueries, suggesting that tool use provides a floor of performance even when visual tokens are uninformative. The persistent gap to the text upper bound likely reflects domain mismatch: code has dense syntactic structure where adjacent blocks are visually near-identical when compressed. No code-specific training data was used; these results are zero-shot transfer from the text QA training set.

## 17 Attention Analysis

### 17.1 Setup Details

Qwen3.5-9B uses a hybrid architecture with 32 decoder layers: 8 standard self-attention layers (at indices 3, 7, 11, 15, 19, 23, 27, 31) and 24 Gated DeltaNet (GDN) linear attention layers. Our attention analysis captures weights from these 8 standard attention layers, as GDN layers do not expose a comparable attention matrix. We toggle the attention implementation from SDPA to eager mode during each decode step so that the forward pass returns full attention weights without modifying the model’s computation. For each generation step, we average the attention distribution across all query heads, then sum within each image’s visual-token range to obtain a per-image attention score. Image-level scores are averaged across generation steps and then across the 8 captured layers.

Because the base model exhibits a positional bias (30% of attention argmax values land on the first image), we report *position-debiased alignment*: the GT-alignment rate macro-averaged across five GT-position quintiles, computed on single-GT samples only. This controls for the correlation between GT image position and the model’s positional attention prior.

### 17.2 Full Attention Shift After Training

Table 16 reports the full segment-level attention breakdown summarized in Figure 5d (§5.2). Six semantic segment types are measured: system prompt, question, tool-call turn (the model’s own tool invocation), tool response (the expanded text), GT images (ground-truth evidence images), and non-GT images (distractor images). The remaining  $\sim 30\%$  of text attention falls on chat-template delimiter tokens (turn separators, generation prompt markers) which act as known attention sinks (Xiao et al., 2023) and are omitted from the table.

The dominant pattern is consistent across all three presets: training redirects attention away from the model’s own tool-call turn ( $-8$  pp), non-GT images ( $-4$  to  $-6$  pp), and the question ( $-1$  pp), and concentrates it on the tool-response text ( $+15$  to  $+16$  pp). This shows that the model learns to read the expanded content rather than re-examining distractors. The shift toward tool-response tokens grows with compression (from 38.2% at  $5\times$  to 41.0% at  $15\times$ ), consistent with the model’s increasing reliance on the text as visual fidelity degrades.

**Table 16** Attention budget shift after training, by input segment and compression preset. The tool-response segment absorbs the largest gain; distractor images show the largest drop.

Segment	5 $\times$			10 $\times$			15 $\times$		
	Base	Trained	$\Delta$	Base	Trained	$\Delta$	Base	Trained	$\Delta$
<i>Text segments</i>									
System prompt	7.0	5.8	-1.2	7.1	6.0	-1.1	7.1	6.5	-0.6
Question	10.1	8.7	-1.4	9.6	8.2	-1.4	10.0	8.7	-1.2
Tool-call turn	16.5	8.3	-8.2	16.0	7.7	-8.3	16.6	8.1	-8.5
Tool response	23.5	38.2	<b>+14.6</b>	26.9	42.0	<b>+15.1</b>	25.2	41.0	<b>+15.8</b>
<i>Vision segments</i>									
GT images	3.0	2.4	-0.6	2.4	1.4	-1.0	2.5	0.8	-1.7
Non-GT images	10.0	5.7	-4.3	8.7	4.3	-4.4	10.0	3.6	-6.4
<i>Total text</i>	87.0	91.9	+4.9	88.9	94.3	+5.4	87.5	95.6	+8.2
<i>Total vision</i>	13.0	8.1	-4.9	11.1	5.7	-5.4	12.5	4.4	-8.2

The vision-to-text shift is not confined to specific layers. Breaking down total vision attention by layer, training reduces the fraction allocated to image tokens at all 8 standard attention layers, with the largest drops in mid-to-late layers (L15–L27,  $-10$  to  $-18$  pp). The drop is also compression-dependent: averaged

across layers, vision attention falls by  $-10$  pp at  $5\times$ ,  $-8$  pp at  $10\times$ , and  $-13$  pp at  $15\times$ , consistent with the model’s increasing reliance on text retrieval as visual fidelity degrades.

## 18 Synthetic Trajectory Examples

This section presents two examples of synthetic trajectories from our training data. In the transcripts below, **blue** highlights image selection references, **green** highlights tool calls, and **red** highlights answer-relevant content.

Single-Hop: HELMET (29 images,  $10\times$  compression)

**Question:** What was the French sounding winner of the 2011 Epsom Derby?

**Gold answer:** **Pour Moi**

[Assistant -- Turn 1]

`<think>`The question asks for the French-sounding winner of the 2011 Epsom Derby, so I need to find the section detailing that specific race’s results. **Image 20** mentions an “iconic image for the 2011 Derby,” which suggests the surrounding images contain the relevant race data. Image 21 discusses a 2003 winner, indicating the document covers multiple years, but **Image 22** explicitly references “first five were Irish-trained” and jockey Seamie Heffernan, which often appears in Derby reports. Given the proximity to the 2011 mention on Image 20 and the specific racing details on Image 22, I will examine Image 22 to locate the winner’s name.`</think>`  
`<tool_call>{"name": "read_text", "arguments": {"image": 22}}</tool_call>`

[Tool Response]

Text content of Image 22: *first five were Irish-trained. Seamie Heffernan won the race at his twelfth attempt [...] [2011 Epsom Derby] 2011 Epsom Derby - The distances between the horses are shown in lengths or shorter; hd = head, nk = neck. Winner details. Further details of the winner, **Pour Moi**: - “Foaled:” 10 January 2008, in Ireland - “Sire:” Montjeu; “Dam:” Gwynn (Darshaan) - “Owner:” Sue Magnier, Michael Tabor and Derrick Smith [...]*

[Assistant -- Final Answer]

`<think>`Scanning the text on this page, I see a specific header for the “2011 Epsom Derby” followed by a section labeled “Winner details.” The text explicitly states, “Further details of the winner, **Pour Moi**,” and lists its foaling date and sire, Montjeu. The name “Pour Moi” fits the description of a French-sounding title, and the context confirms it is the winner of the specified race.`</think>` **pour moi**

**Single-Hop Example Analysis.** The model selects Image 22 (out of 29) on its first attempt by leveraging coarse visual cues from the compressed overview. A single EXPAND call suffices, and the reasoning trace cites specific retrieved evidence (“Further details of the winner, Pour Moi”) rather than paraphrasing, confirming that the trace generator grounds conclusions in tool-response content.

Multi-Hop: MuSiQue (23 images,  $5\times$  compression)

**Question:** What is the area code for Cincinnati in the state where Lewis Kemp House is located?

**Gold answer:** **513**

**Hops:** Lewis Kemp House → Ohio → Cincinnati area code

[Assistant -- Turn 1]

`<think>`The question asks for the area code for Cincinnati in the state where the Lewis Kemp House is located. I need to first determine the state associated with the Lewis Kemp House to narrow down the geographic context. The thumbnail for **Image 16** mentions “first woman judge,” which might be part of a biographical entry that includes location details relevant to the house or the region. I will read Image 16 to see if it contains information linking the Lewis Kemp House to a specific state.`</think>` `<tool_call>{"name": "read_text", "arguments": {"image": 16}}</tool_call>`

[Tool Response]

Text content of Image 16: [...] *[Lewis Kemp House] The Lewis Kemp House is a historic pioneer farmstead in the city of Dayton, Ohio, United States. Built for one of the area's earliest residents, it was a religious center in its first years, while later years saw its expansion to its present form. Now located among much newer houses, it is Dayton's oldest surviving residence, and it has been named a historic site. [...]*

[Assistant -- Turn 2]

<think>Image 16 confirms that the Lewis Kemp House is located in “Dayton, Ohio, United States.” This establishes that the relevant state is Ohio. Now I need to find the area code for Cincinnati within Ohio. The thumbnail for Image 22 mentions “Langdon House” which is a historic house, and it is possible that nearby entries contain information about Ohio area codes. I will read Image 22.</think> <tool\_call>{"name": "read\_text", "arguments": {"image": 22}}</tool\_call>

[Tool Response]

Text content of Image 22: *[Langdon House] The Langdon House is a historic house on the eastern side of Cincinnati, Ohio, United States. [...] [List of Ohio area codes] Code Created Region 216 1947 Cleveland (October 1947) 234 2000 Akron, Canton, Youngstown, and Warren, overlay with 330 [...] 419 1947 Northwest and north central Ohio including...*

[Assistant -- Turn 3]

<think>Image 22 contains the beginning of a list of Ohio area codes but is cut off before reaching Cincinnati. The list continues on Image 23, which should contain the Cincinnati entry. I will read Image 23 to find the specific code.</think> <tool\_call>{"name": "read\_text", "arguments": {"image": 23}}</tool\_call>

[Tool Response]

Text content of Image 23: *Toledo, Sandusky, and Ashland, overlay with 567 [...] 513 1947 Southwest Ohio including Cincinnati (October, 1947) 567 1947 Northwest and north central Ohio including Toledo [...]*

[Assistant -- Final Answer]

<think>Image 22 establishes that Cincinnati is in Ohio, confirming the state context. Image 23 contains the list of Ohio area codes, specifically stating “513 1947 Southwest Ohio including Cincinnati.” By combining the location from Image 16 (Lewis Kemp House in Ohio) and the area code data from Image 23, the answer is 513.</think> **513**

**Multi-Hop Example Analysis.** This trajectory demonstrates multi-hop compositional reasoning: the model decomposes the question into sub-problems, selecting a different image for each (Images 16, 22, 23). Each EXPAND call retrieves one piece of the reasoning chain, and the final answer synthesizes evidence from all three.

## 19 Prompts

This section lists all prompts used in our pipeline. The EXPAND tool is implemented as `read_text` in text prompts and `zoom_in` in image prompts.

### Text Retrieval System Prompt

You are a helpful assistant that answers questions based on rendered text images. You can view the images and use the `read_text` tool to read the actual text content of any image for detailed analysis.

You have a tool called `read_text` that reads the text content of any image. To use it:

```
<tool_call>{"name": "read_text", "arguments": {"image": IMAGE_NUMBER}}</tool_call>
```

You can call `read_text` multiple times on different images. Always reason inside `<think>` and `</think>` tags before taking any action. If you need more detail from a specific image, call `read_text` to get its text content.

Do not read the entire input — only read images that are likely relevant. Once you have enough information, provide your final answer.

### Image Zoom System Prompt

You are a helpful assistant that answers questions about multi-image documents. You can view low-resolution thumbnail images and use the `zoom_in` tool to get the original full-resolution image for detailed analysis. You have a tool called `zoom_in` that shows the original image at full resolution. Images are numbered starting from 1. To use it:

```
<tool_call>{"name": "zoom_in", "arguments": {"image": IMAGE_NUMBER}}</tool_call>
```

You can call `zoom_in` multiple times on different images. Always reason inside `<think>` and `</think>` tags before taking any action. First examine the thumbnail images to identify which ones likely contain relevant information, then call `zoom_in` to get the original full-resolution version. Once you have enough information, provide your final answer.

### Trace-Generation System Prompt

You generate training data for a document QA model. Output ONLY the requested format with `--RESPONSE{N}--` delimiters. Start your output directly with `--RESPONSE1--`. No preamble.

**ROLEPLAY CONSTRAINT (CRITICAL):** You are roleplaying a model that is solving the question from scratch by investigating the document. The `<think>` blocks must read as genuine first-person investigation of the image content. NEVER reference these prompt elements inside `<think>`: “the answer”, “the answer key”, “the provided answer”, “ground truth”, “the prompt says/states/mentions/indicates/asks”, “the question’s premise”, “the task says”, “training data/example”, “provided text snippets”, or any phrasing that implies you were told the answer or the correct image in advance. Treat the answer as something you DISCOVER by reading, not something you were given. Do not include “wait, re-reading” or “there seems to be a mismatch” style self-correction — write the reasoning as if it landed correctly the first time.

**STYLE:** Each `<think>` block is 3–5 sentences. After-zoom reasoning MUST quote or cite specific word/s/phrases from the `tool_response` text. Do not fabricate text that isn’t in the `tool_response`.

### LLM Judge Prompt

You are an expert evaluator. Determine if the model’s answer correctly answers the question based on the gold answers.

```
[QUESTION]
{question}
[/QUESTION]
[GOLD ANSWERS]
{gold_answers}
[/GOLD ANSWERS]
[MODEL ANSWER]
{model_answer}
[/MODEL ANSWER]
```

Evaluation criteria:

- The answer must convey the same core meaning as the gold answers
- Partial matches should be marked incorrect
- Additional correct information beyond gold answers is acceptable
- Empty or off-topic responses are incorrect
- Minor formatting differences (e.g., “10:30 pm” vs “10:30 p.m.”) should be accepted

Respond with ONLY `[[YES]]` if the model answer is correct, or `[[NO]]` if incorrect.